Journal of Advanced Research xxx (xxxx) xxx

Contents lists available at ScienceDirect

Journal of Advanced Research

journal homepage: www.elsevier.com/locate/jare

Alisol B 23-acetate broadly inhibits coronavirus through blocking virus entry and suppresses proinflammatory T cells responses for the treatment of COVID-19

Qiaohui Du [a,b,1], Ronghui Liang [c,1], Meiling Wu [a], Minxiao Yang [a], Yubin Xie [c], Qing Liu [a], Kaiming Tang [c], Xiang Lin [a], Shuofeng Yuan [c,d,e,*], Jiangang Shen [a,b,*]

[a] School of Chinese Medicine, Li Ka Shing Faculty of Medicine, The University of Hong Kong, 3 Sassoon Road, Pokfulam, Hong Kong, Hong Kong Special Administrative Region
[b] State Key Laboratory of Pharmaceutical Biotechnology, The University of Hong Kong, Pokfulam, Hong Kong, Hong Kong Special Administrative Region
[c] State Key Laboratory of Emerging Infectious Diseases, Department of Microbiology, Li Ka Shing Faculty of Medicine, The University of Hong Kong, Pokfulam, Hong Kong Special Administrative Region
[d] Centre for Virology, Vaccinology and Therapeutics, Hong Kong Science and Technology Park, Hong Kong Special Administrative Region
[e] Department of Clinical Microbiology and Infection Control, The University of Hong Kong-Shenzhen Hospital, Shenzhen, Guangdong, China

HIGHLIGHTS

- This study developed a novel therapeutic agent alisol B 23-acetate for COVID-19 treatment.
- Alisol B 23-acetate has inhibitory effects on different species of coronavirus including MERS-CoV, SARS-CoV-2, SARS-CoV-2.B.1.1.7 lineage (*Alpha* variant), B.1.617.2 lineage (*Delta* variant), B.1.1.529 lineage (*Omicron* variant) and Omicron BA.5.2 lineage.
- Alisol B 23-acetate has inhibition potency toward ACE2.
- Alisol B 23-acetate protects against SARS-CoV-2 and its variants challenge in several animal models.
- Alisol B 23-acetate also shows anti-inflammation activities *in vivo* and *in vitro*.

GRAPHICAL ABSTRACT

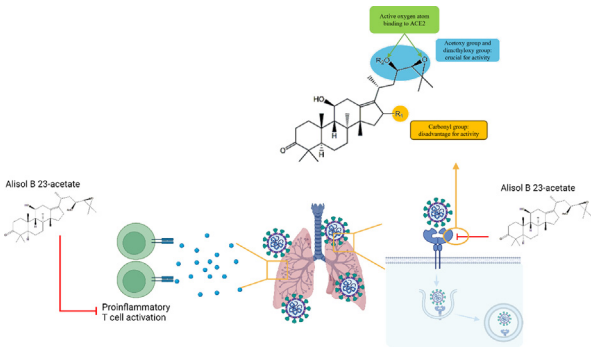

ARTICLE INFO

Article history:
Received 30 March 2023
Revised 11 September 2023
Accepted 2 October 2023
Available online xxxx

Keywords:
Alisol B 23-acetate
Anti-coronavirus

ABSTRACT

Introduction: Emerging severe acute respiratory syndrome (SARS) coronavirus (CoV)-2 causes a global health disaster and pandemic. Seeking effective anti-pan-CoVs drugs benefit critical illness patients of coronavirus disease 2019 (COVID-19) but also may play a role in emerging CoVs of the future.
Objectives: This study tested the hypothesis that alisol B 23-acetate could be a viral entry inhibitor and would have proinflammatory inhibition for COVID-19 treatment.
Methods: SARS-CoV-2 and its variants infected several cell lines were applied to evaluate the anti-CoVs activities of alisol B 23-aceate *in vitro*. The effects of alisol B 23-acetate on *in vivo* models were assessed by using SARS-CoV-2 and its variants challenged hamster and human angiotensin-converting enzyme 2

* Corresponding authors.
E-mail addresses: yuansf@hku.hk (S. Yuan), shenjg@hku.hk (J. Shen).
[1] These authors contributed equally: Qiaohui Du and Ronghui Liang.

https://doi.org/10.1016/j.jare.2023.10.002

Please cite this article as: Q. Du, R. Liang, M. Wu et al., Alisol B 23-acetate broadly inhibits coronavirus through blocking virus entry and suppresses proinflammatory T cells responses for the treatment of COVID-19, Journal of Advanced Research, https://doi.org/10.1016/j.jare.2023.10.002

COVID-19
Anti-immunoinflammatory activity
ACE2

(ACE2) transgenic mice. The target of alisol B 23-acetate to ACE2 was analyzed using hydrogen/deuterium exchange (HDX) mass spectrometry (MS).

Results: Alisol B 23-acetate had inhibitory effects on different species of coronavirus. By using HDX-MS, we found that alisol B 23-acetate had inhibition potency toward ACE2. *In vivo* experiments showed that alisol B 23-acetate treatment remarkably decreased viral copy, reduced $CD4^+$ T lymphocytes and $CD11b^+$ macrophages infiltration and ameliorated lung damages in the hamster model. In *Omicron* variant infected human ACE2 transgenic mice, alisol B 23-acetate effectively alleviated viral load in nasal turbinate and reduced proinflammatory cytokines interleukin 17 (IL17) and interferon γ (IFNγ) in peripheral blood. The prophylactic treatment of alisol B 23-acetate by intranasal administration significantly attenuated *Omicron* viral load in the hamster lung tissues. Moreover, alisol B 23-acetate treatment remarkably inhibited proinflammatory responses through mitigating the secretions of IFNγ and IL17 in the cultured human and mice lymphocytes *in vitro*.

Conclusion: Alisol B 23-acetate could be a promising therapeutic agent for COVID-19 treatment and its underlying mechanisms might be attributed to viral entry inhibition and anti-inflammatory activities.

Introduction

Within two decades, the world has experienced three major outbreaks of coronavirus (CoVs) disease (COVID), including severe acute respiratory syndrome (SARS), middle east respiratory syndrome (MERS) and COVID 2019 (COVID-19) [1–3]. With rapid transmission and high mutation of SARS-CoV-2, the COVID-19 pandemic has made much higher public health disasters and economic damages than SARS-CoV and MERS-CoV pandemics. Coronavirus infects human through receptor-binding domain (RBD) of spike protein binding to the angiotensin-converting enzyme 2 (ACE2) receptor. Until now, 12 different important variants have been identified including B.1.1.7 (*Alpha*), B.1.351 (*Beta*), B.1.525 (*Eta*), B.1.427/B.1.429 (*Epsilon*), B.1.526 (*Iota*), B.1.617.1 (*Kappa*), B.1.617.2 (*Delta*), C.37 (*Lambda*), P.1 (*Gamma*), P.2 (*Zeta*), P.3 (*Theta*) and B.1.1.529 (*Omicron*) [4–8]. Recently, *Omicron* and its variants become the most popular SARS-CoV-2 variants. The *Omicron* variants obtain larger numbers of mutations in RBD region and have high affinity to bind human receptor ACE2 [9]. Meanwhile, the mutation in RBD of *Omicron* variants exhibits the increased antibody evasion, leading the rapid spread of the *Omicron* variants [10]. With its high transmissibility, the *Omicron* variants have rapidly replaced *Delta* as the dominant variants globally. Under the global application of multiple COVID-19 vaccinations, *Omicron* variant infection appears to have the attenuated symptoms and mortality. However, the aged patients with *Omicron* infection still suffer from severe lung inflammation and other complications, leading to the increase of mortality.

Scientists has made great effects to seek effective drugs for COVID-19 treatment. Remdesivir, hydroxychloroquine and lopinavir-ritonavir were initially developed for COVID-19 treatment with pan-coronavirus inhibitory effects, but their clinical effectiveness were unsatisfactory and controversial [11–15]. Combination treatment of interleukin-6 receptor inhibitors tocilizumab and sarilumab were studied to increase survival rates in severe COVID-19 patients [16]. Paxlovid (nirmatrelvir plus ritonavir), the SAR-CoV-2 main protease inhibitor, revealed antiviral activities and reduced the risk of critical illness or death [17–19]. However, Paxlovid treated COVID-19 patients showed greater incidence of viral rebound than the untreated *Omicron* variant infected patients [20]. Notably, SARS-CoV-2 *Omicron* variant exerts drug resistances [20] and have antibody evasion [21]. With potential new emerging variants and/or newly species in the future, developing potential therapeutic agent against SARS-CoV-2 and its mutants are urgent needed for drug discovery to COVID-19 treatment.

Natural medicinal compounds are important sources for drug discovery. Traditional Chinese Medicine (TCM) has long history against epidemic infective diseases. In China, several TCM formulae are recommended as potential therapeutic agents but the scientific basis and effectiveness remain to be explored. QingFei PaiDu (QFPD) Decoction is one of the representative herbal prescriptions recommended for COVID-19 treatment in China. A recent review and meta-analysis suggests the effectiveness and safety of QFPD as an adjunct therapy with conventional treatment against COVID-19 [22]. Several antiviral and anti-inflammation compounds including Oroxylin A, hesperetin, scutellarin, glycyrrhizic acid and glycyrrhizin, were identified from the QFPD [23–25]. The triterpenoids licorice-saponin A3 and glycyrrhetinic acid from licorice were reported to inhibit SARS-CoV-2 infection by targeting spike protein of SARS-CoV-2 [26]. Thus, we initially tested 35 active compounds from QFPD with potentials of anti-viral, anti-inflammation and immunomodulation for screening anti-coronavirus compounds based on the literatures [23–25,27–30]. We found alisol B 23-acetate, an active compound from *Alismatis Rhizoma,* showed inhibitory effects on SARS-CoV-2 infection *in vitro* (**Fig. S1**). Alisol A/B/C and their acetate derivatives are the major bioactive compounds among triterpenoid compounds of *Alismatis Rhizoma* [31]. Alisol A and alisol B 23-acetate have antibiotic bioactivities [32]. Alisol B 23-acetate also reveals the anti-cancer, anti-inflammation and hepatoprotective properties [33–35]. *Alisma* herb extract and its ingredient alisol B 23-acetate could attenuate allergic asthma and lipopolysaccharide-induced acute lung injury [36,37]. It is of interesting to explore the potentials of Alisol A/B/C and their acetate derivatives for COVID-19 treatments.

The aim of this investigation was designed to develop a novel therapeutic agent for COVID-19 treatment. In the present study, we performed a series of experiments to test the hypothesis that alisol B 23-acetate could be a promising antiviral compound against COVID-19 via viral entry inhibition and anti-inflammatory activities.

To fully achieve the anti-CoVs activities of alisol B 23-acetate, we tested inhibitory effects of alisol B 23-acetate on different species of coronavirus lineages *in vitro* firstly. We adopted pseudotyped Vesicular Stomatitis Virus (VSV) and receptors overexpressed cells to explore the potential mechanisms of alisol B 23-acetate in viral entry. HDX-MS techniques were utilized to verify the molecular interaction between alisol B 23-acetate and ACE2 receptor. To identification of alisol B 23-acetate for COVID-19 treatment, several coronaviruses challenged animal models were established to evaluate the role of alisol B 23-acetate in ameliorating lung damage and inflammation caused by virus. The potential drug alisol B 23-acetate could benefit critical illness patients of COVID-19 but also may play a role in new emerged CoVs variants in the future.

Materials and methods

Cell culture

Human epithelial colorectal adenocarcinoma cells (ATCC, Caco-2), African green monkey kidney cells, clone E6 (ATCC, Vero E6) and adenocarcinoma human alveolar basal epithelial cells expressing human ACE2 and human TMPRSS2 (InvivoGene, A549-ACE2-TMPRSS2) were applied for antiviral studies. Vero E6 cells stably expressed TMPRSS2 and HEK293 cells (ATCC) stably expressed hACE2 were generated by transducing lentivirus and followed by puromycin selection. All cells were maintained in DMEM supplemented with 10 % FBS, 50 U/ml penicilin and 50 μg/ml streptomycin.

Virus

The SARS-CoV-2 HKU-001a strain (GenBank accession number: MT230904) and *Omicron* B.1.1.529 lineage (GenBank: OM212472) were isolated from the nasopharyngeal aspirate specimen of laboratory-confirmed COVID-19 patients in Hong Kong [38,39]. The MERS-CoV (HCoV-EMC/2012) was a gift from Dr. Ron Fouchier. The *Alpha* variant (GenBank: OM212469), *Delta* variant (GenBank: OM212471), and *Omicron* BA.5.2. (GISAID accession: EPI_ISL_13777658) were archived in Department of Microbiology, The University of Hong Kong. All viral associated experiments involving live SARS-CoV-2, *Alpha* variant, *Delta* variant, *Omicron* variant and MERS-CoV were conducted in the Biosafety Level 3 Facility at the University of Hong Kong and used the standard operating procedures as our previous report [40].

Antiviral assay in vitro

Caco-2 cells and VeroE6 were infected with SARS-CoV-2 HKU-001a, *Alpha* variant, *Delta* variant, *Omicron* variant, and MERS-CoV with 0.1 multiplicity of infection (MOI). After 1 h of infection, the inoculum was removed, and the cells were washed with PBS. Alisol A, alisol B, alisol C and their derivatives were purchased from commercial company with purity $\geq$ 98 % (Chengdu Push Biotechnology). The chemicals were dissolved in DMSO for treatment. Cell viabilities of A549, Caco-2 and VeroE6 were detected by 3-(4,5-di methylthiazol-2-yl)-2,5-diphenyltetrazolium bromide (MTT) after 48 h treatment with alisol B 23-acetae at 5, 10, 20, 40, 60 μM. Supernatants and cell lysis were collected at 24- or 48-hours post inoculation (hpi) for plaque assays and quantitative real-time PCR assay (qRT-PCR). Viral loads of MERS-CoV, SARS-CoV-2, *Alpha* variant, *Delta* variant and *Omicron* variant were determined by qRT-PCR. The primers and probe sequences used for viral load detection were showed in Table S1.

Pseudotype-based vesicular stomatitis virus assay

As previous report, SARS-CoV-2 and its variants spike protein pseudotyped Vesicular Stomatitis Virus (VSV) were generated with small modifications [41]. In detail, BHK-21/WI-2 cells (Kerafast) overexpressing with spike proteins were inoculated with VSV-G psedutyped ΔG-luciferase VSV (Kerafast). After 24 h VSV-G antibody (I1, ATCC) inoculation, pseudotyped particles were collected by removing cell debris and stored at −80 °C until use. SARS-CoV-2 *Omicron* variant spike fluc pseudovirus were purchased from Quimigen (PSSO-HLA003). In viral entry test, A549-ACE2-TMPRSS2 cells and HEK293-hACE2 were treated with alisol B 23-acetate at 12.5, 25, 50 μM for 1 h prior to inoculation with respective pseudotyped VSV. After treated with alisol B 23-acetate for 1 h, the cells were refed with fresh culture medium. At 24 h post-transduction, we quantitatively determined the firefly luciferase activity by using bright-Glo™ luciferase assay (Promega).

Virus attachment assay

We tested the role of alisol B 23-acetate on virus-cell attachment applying SARS-CoV-2 and VeroE6 cells. Three doses of alisol B 23-acetate were pre-incubated with VeroE6 cells at 2 h before virus infection at 12.5, 25, 50 μM. After 2 h of alisol B 23-acetate treatment, SARS-CoV-2 virus were inoculated into cells with MOI at 5. The cells were incubated at 4 °C for 1.5 h to allow the virus attachment. After 1.5 h post-transduction, the cells were collected and staining with spike protein of SARS-CoV-2 for flow cytometry analysis.

HDX-MS analysis

HDX-MS analysis was performed to investigate the binding potentials of alisol B 23-acetate to ACE2 according to the protocol as previous report with minor modifications [42]. ACE2 protein was purchased from Genescript Biotech Corp (NP_068576.1, residues 18–740) and dissolved in phosphate buffer at 20 μM. Alisol B 23-acetate was dissolved in 15 % ethanol and reacted with ACE2 at 9:1 in a 10 μL solution system. Deuterium exchange was initiated protein sample with 30 μL D_2O phosphate buffer (pD 7.4). After exchanged for 1, 10 and 60 min, the mixtures were analyzed by HDX-MS using Waters ACQUITY UPLC system equipped with Waters Synapt G2-Si mass spectrometer. The experiments were performed with following parameters: capillary voltage, 3500 V; source temperature, 150 °C; desolvation temperature, 350 ℃. Scan range was set from m/z 100 to m/z 2000 with accurate mass measurement for all mass peaks. The digestion column was Waters Enzymate BEH-Pepsin column followed by Waters ACQUITY UPLC Protein BEH C4 Column before MS analysis. The mobile phase consisted of 0.1 % formic acid (FA) water (A) and 0.1 % FA acetonitrile (B) by using gradient elution of 0–5 min, 20–80 %ACN; 5–8 min, 80 % ACN; 8–10 min, 80–20 % ACN. Peptide was generated by ProteinLynx Global Server (PLGS, Waters) and processed using DynamX 3.0 (Milford, Massachusetts). The average mass error of all peptides was below 3 ppm for analysis and the maximum mass error was set at 10 ppm. The standard deviation of retention time was below 5 %. Crystal structure of ACE2 was obtained from Protein Data Bank (PDB ID:1r42). The difference in deuterium uptake over 95 % confidence interval was regarded as significant change for HDX.

T lymphocytes culture and treatment

Human T cells were isolated from peripheral blood mononuclear cells (PBMC) of health doners and sorted by human CD4 microbeads and magnetic-activated cell sorting method (MACS) according to our previous protocol with minor modification [43]. Mouse T lymphocytes were collected from lymph nodes and spleens by using mouse CD4 microbeads. Anti-CD3 and anti-CD28 antibodies were pre-coated for activation and expansion of human T cells. Carboxyfluorescein succinimidyl ester (CFSE), a fluorescent tracking dye, was used to staining the T cells for proliferation test. After CFSE staining, the proliferation of T lymphocytes was analyzed by flow cytometry. NovoCyte Quanteon flow cytometer (Agilent) was used to test the conjugated fluorochromes and software FlowJo was used for data analysis. We also detected the activities of alisol B 23-acetate on the differentiation of T cells. Th17 cells were induced by TGFβ, IL6 and anti-IFNγ antibody. Th1 cells were stimulated by IL12. Tfh cells were derived by IL6 and IL21 stimulation. The Th17, Th1 and Tfh cells were sorted from $CD4^+$ T cells by MACS. For cytokines analysis, culture medium was

collected to detect the release of IL17 and IFNγ within 3 days by Elisa kit (Biolegend). To enrich the cytokines in the culture supernatant, we freeze-dried culture medium and dissolved in 100 μL distilled water for testing. The antibodies for lymphocytes flow cytometry analysis and the Elisa kit for cytokines analysis were listed in Table S1.

Antiviral experiments in hamster and hACE2-mice

Both male and female Syrian hamsters aged 6–10 weeks old were obtained from the Chinese University of Hong Kong Laboratory Animal Service Centre. Heterogenous K18-hACE2 C57BL/6J mice (2B6.Cg-Tg(K18-ACE2)2Prlmn/J), male and female, aged 6–8 weeks, were purchased from Jackson Laboratory. The animals were kept at biosafety level 2 for housing and given standard pellet feed and water ad libitum as previously described [38]. The hamsters were infected with SARS-CoV-2, *Delta* variant or *Omicron* variant based on different experimental protocols. In SARS-CoV-2 and *Delta* variant experiments, each hamster was intranasally inoculated with 10^4 PFU of SARS-CoV-2 or *Delta* variant in 100 μL PBS under intraperitoneal ketamine and xylazine anesthesia (ketamine 5 mg/kg and xylazine 120 mg/kg for hamster). In *Omicron* BA.5.2 experiments, both hamsters and hACE2-mice were inoculated with 10^5 PFU of *Omicron* BA.5.2 (ketamine 5 mg/kg and xylazine 100 mg/kg for mice). Furthermore, we specifically evaluated the prophylactic and therapeutic effects of alisol B 23-acetate against SARS-CoV-2 *Omicron* variant infections. The hamsters were allocated with three groups including mock infection, viral infection with vehicle treatment, and viral infection with alisol B 23-acetate treatment. Alisol B 23-acetate (180 mg/ml) was dissolved in a solvent solution containing ethanol (Sigma), polyethylene glycol 400 (Sigma, PEG400) and saline (10:3:2) while the same solvent solution without alisol B 23-acetate was used as vehicle treatment. All solutions were filtered by 0.22 μM filter. In prophylactic protocol, prior to *Omicron* variant infection, the hamsters were intranasally (i.n.) administrated with 40 μL of alisol B 23-acetate solution corresponding to the dosage of 60 mg/kg. In therapeutic protocols, after infected with SARS-CoV-2 and *Delta* variant at 24 h, the hamsters were intraperitoneally injected with the same dosage of alisol B 23-acetate solution (60 mg/kg) at 1, 2, 3 dpi (Fig. 4A). In *Omicron* variant infection experiments with therapeutic protocols, alisol B 23-acetate was sustained for 2 days with the same dosage to the mice because of the short pathogenic period of *Omicron* variant infection (Fig. 6A). In prophylactic protocol, prior to *Omicron* variant infection, the hamsters were intranasally (i.n.) administrated with 40 μL of alisol B 23-acetate solution corresponding to the dosage of 60 mg/kg (Fig. 6A). At the designed time-points, the hamsters were sacrificed at 4 dpi for virological and histopathological examinations. Viral yield and gene expression levels in lung tissues were detected by RT-qPCR methods. The primers for inflammation cytokines were shown in the Table S1. ELISA kit was used to detect the levels of cytokines in the sera according to the manufacture's recommendations (hamster IFNγ: MyBiosource). The pathology of viral infected hamster lung tissues was examined by Hematoxylin and Eosin (H&E) staining in accordance with our established protocol [40,44,45].

Ethics statement

All animal care and experimental procedures were approved by the University Committee on the Use of Live Animals in Teaching and Research in the University of Hong Kong (Reference code: CULATR no. 5838-21).

Endogenous ROS and peroxynitrite staining

We collected fresh lung tissue (~1 cm^2) at 4 days after vehicle or alisol B 23-acetate treatment. To detect the antioxidant activity, we used HKYellow (20 μM) [46] and hydroethidine (HEt 20 μM; Invitrogen) to measure the productions of peroxynitrite ($ONOO^-$) and superoxide (O_2^-), respectively. Lung tissues were stained with HKYellow and HEt for 2 h prior to fixation. After staining, fresh lung samples were sectioned into 20 μm cryosection slices for imaging study. The confocal images were detected by microscope (Zeiss LSM 800, Germany; Core facility in LSK Faculty of Medicine, HKU). The quantified fluorescent intensity was analyzed by using ImageJ software.

Transcriptome analysis

Lung RNA samples were used for RNA-seq reads and checked by FastQC (v0.11.7). Library construction was performed using Nextera XT kit following the manufacture's protocol. For RNA sequencing of the SARS-CoV-2 infected samples, DNBSEQ method was adopted to repair the RNA samples and library construction. By using Cutadapt version 1.16, we selectively picked the reads at the length $\geq$ 30 that were recognized as high-quality reads and removed low quality reads and adapter contamination. The transcriptome alignment/mapping to each gene were done using TopHat version 2.1.1 with default parameters. All the samples had over 80 % mapping with hamster reference MesAur 2.0 (GCA_017639785.1) downloaded from Ensemble. Cut-off criteria for low expression gene with CPM threshold value of 1 were filtered out using limma-voom. Read counts were normalized by trimmed mean of M-values method and the differentially expressed genes were calculated using R package edgeR (v3.28.1). The value of False Discovery Rate (FDR) $\leq$ 0.05 was considered as differential gene expression level. The enriched pathway analysis was conducted and generated by R package clusterProfiler42 (v3.14.3). R package pheatmap (v1.0.12) model was applied to generate heatmaps. R package version 0.7.7.

Immunofluorescence

The collected lung tissue was post-fixed with 4 % PFA for 48 h and dehydrated in 30 % sucrose solution. The lung tissue was embedded in O.C.T. and cut into 25 μm sections for antigen-retrieve and immunofluorescence staining. The antigen-retrieved process was conducted by heating samples in citrate acid buffer (pH 6.0). PBS buffer containing 5 % goat serum was utilized for blocking. Then. the samples were stained with specific primary antibodies and secondary antibodies, counterstained the nucleus with DAPI. Cell images were obtained by confocal microscope (Zeiss LSM 800, Germany; Core facility in LSK Faculty of Medicine, HKU). Specific primary antibodies were shown in Table S1.

Statistical analysis

The data were presented as the Mean ± S.E.M and statistical analysis were conducted by using One-way ANOVA followed by Dunnett's multiple-comparison test for multiple group comparisons. Unpaired two-tailed Student's *t*-test was performed to compare the statistical difference between two groups. P-value less than 0.05 was considered as statistical significance.

Results

Alisol B 23-acetate has pan-coronavirus inhibitory properties by targeting ACE2

We firstly screened the anti-viral activities of 35 constituents from QFPD on inhibiting SARS-CoV-2 infection in Caco2 cells (**Fig. S1**). Among these compounds, alisol B 23-acetate was the only one showing the inhibitory effects on the viral titer in the cultured supernatant. Next, we examined the antiviral activities of alisol A/B/C and their acetate derivatives by using *Omicron* BA.5.2 variant infected Caco2 cells (Fig. 1**a and 1b**). Both alisol B and alisol B 23-acetate dose-dependently decreased the *Omicron* variant copies in the cell culture supernatant (Fig. 1**b**). Alisol B 23-acetate reduced ~ 1-log10 viral titer at 10 μM in the supernatant. Interestingly, alisol A, alisol C and their derivatives had no inhibitory effect on the viral copies. Meanwhile, alisol B 23-acetate had lesser cytotoxicity than alisol B (Fig. 1**c**). The 50 % cytotoxicity concentrations (CC50) of alisol B and alisol B 23-acetate were at 8.1 μM and 22.46 μM, respectively (Fig. 1**c**). The CC50 of alisol B 23-acetae to A549 cell line was at 46.14 μM (**Fig. S2**). Those data suggest that alisol B 23-acetate could be a promising compound with anti-SARS-CoV-2 and less cytotoxicity. The safety was further confirmed by acute toxicity test using the golden Syrian hamsters *in vivo*. The hamsters were intraperitoneally injected 360 mg/kg which was six-time higher than the therapeutic dosage in the animal experi-

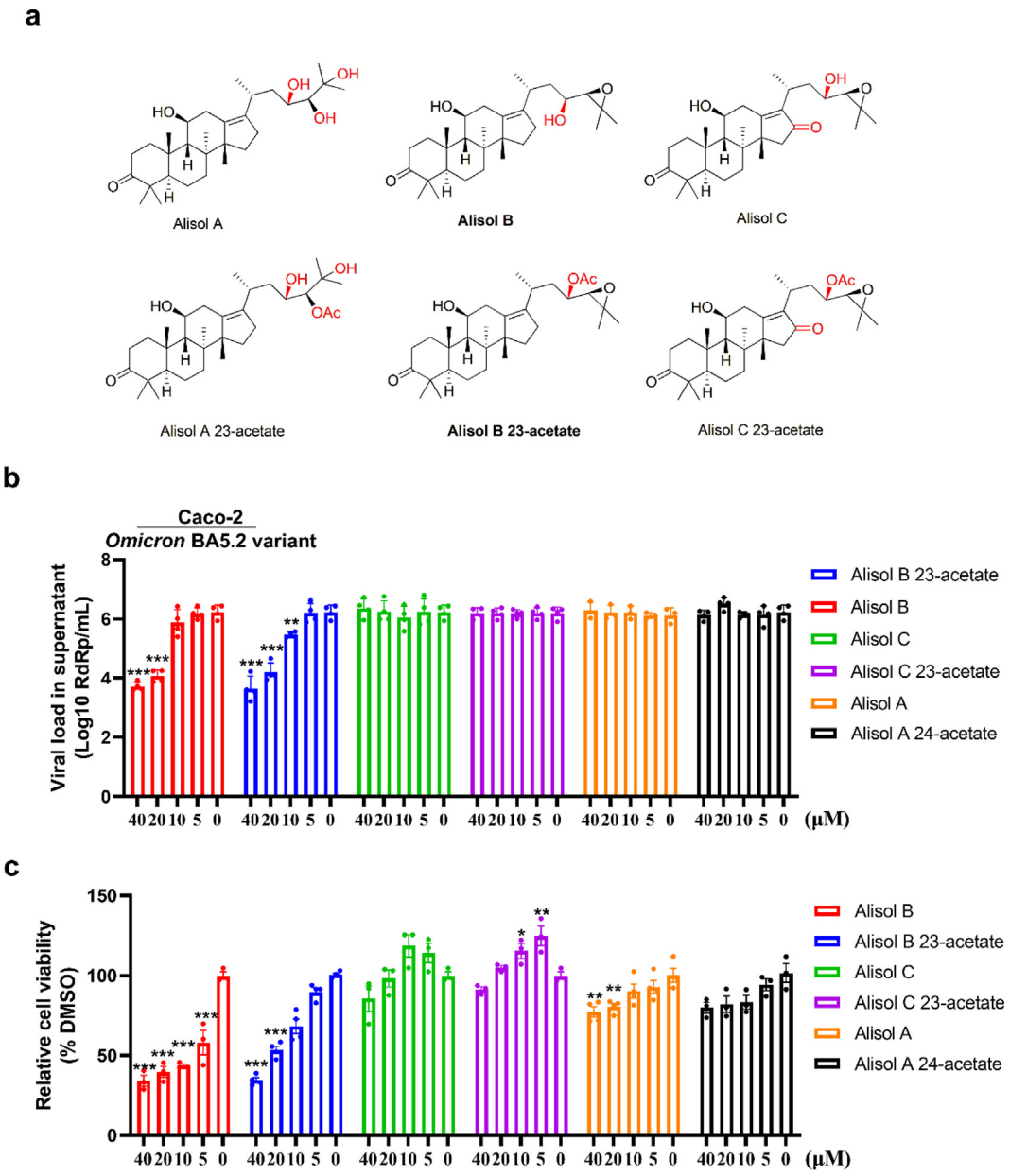

Fig. 1. The antiviral activities and cytotoxicity of alisol B 23-acetate (23-alisol B) and its derivatives. Caco-2 cell line was infected with *Omicron* variant (multiplicity of infection (MOI) = 0.5) and treated with compounds in 4 dosages (5, 10, 20, 40 μM). (**a**) Chemical structure of 23-alisol B and its derivatives. (**b**) Virus loads in the cell culture supernatant were determined by qualitative polymerase chain reaction with reverse transcription at 48 h.p.i. and normalized by human β-actin (n = 3 for each group, **p = 0.0083 for 10 μM 23-alisol B relative to DMSO group). (**c**) Caco-2 cell viabilities were tested by 3-(4,5-dimethylthiazol-2-yl)-2,5-diphenyltetrazolium bromide (MTT) assay (n = 3 for each group, *p = 0.0434, **p = 0.0025 for alisol C 23-acetate; **p = 0.0068 for 5 μM alisol A, **p = 0.0019 for 10 μM alisol A). All the data are presented as mean ± S.E.M (***p < 0.001, all comparations relative to DMSO group, one-way ANOVA followed by Dunnett test). All experiments were performed in n = 3 biological replicates and repeated twice for confirmation.

ments. The results revealed that alisol B 23-acetate had no influence on body weight (Fig. S3**a**), organ index, liver functions (Fig. S3**b and S3c**) and morphological change (Fig. S3**d**). Thus, alisol B 23-acetate has been specifically selected for further investigation.

We next examined the inhibitory effects of alisol B 23-acetate on different coronavirus species including MERS-CoV, SARS-CoV-2, *Alpha* variant, *Delta* variant, *Omicron* variant BA.1. and BA.5.2 by using Caco-2 cells and A549-TMPRSS2. From the results, alisol B 23-acetate dose-dependently decreased the viral yields of MERS-CoV, SARS-CoV-2, *Alpha* variant, *Delta* variant and *Omicron* variant in the culture supernatants of the Caco-2 cells (Fig. 2**a-2f**). At 30 μM, alisol B 23-acetate reduced MERS-CoV viral titer by ∼ 1-log10, that of ∼ 2-log10 and ∼ 3-log10 for *Alpha* and *Delta*, respectively. As for *Omicron* BA1.1 variant, alisol B 23-acetate at 10 μM exhibited to markedly decrease viral copies by ∼ 1.5-log10 (Fig. 2**e**). Meanwhile, alisol B 23-acetate at 10 μM subtracted viral yields by ∼ 0.5-log10 in the *Omicron* BA.5.2 infected A549-TMPRSS2 cells (Fig. 2**f**). Furthermore, at the dosages of 30 μM and 40 μM, alisol B 23-acetate completely inhibited intracellular viral loads in the cells. The IC_{50} values for MERS-CoV, SARS-CoV-2, *Alpha* and *Delta* were at 8.3, 15.02, 12.02, 19.29 μM, respectively (Fig. 2**g-2k**) and for *Omicron* BA.5.2 was at 11.09 μM (Fig. 2**l**). The selectivity index (SI) values were calculated to measure the window between cytotoxicity and antiviral activity through dividing CC50 by IC50. The SI values of alisol B 23-acetate for MERS-CoV, SARS-CoV-2, *Alpha*, *Delta*, *Omicron* BA1.1 and *Omicron* BA5.2 were at 2.7, 1.50, 1.86, 1.16, 1.42 and 4.16 respectively. Those results suggest that alisol B 23-acetate has broad anti-coronavirus bioactivities.

To explore the antiviral mechanisms, we investigated the roles of alisol B 23-acetate on viral entry by utilizing vesicular stomatitis virus (VSV)-based wild type and *Omicron* variant spike (S) pseudotyped virions. Alisol B 23-acetate significantly decreased the entry of SARS-CoV-2 S pseudotyped virions to VeroE6 cells, A549-ACE2-TMPRSS2 cells and VeroE6-TMPRSS2 cells (Fig. 3**a-3c**). Camostat, a TMPRSS2 inhibitor, abated virus entry to VeroE6-TMPRSS2 cells and decreased S pseudotyped virions entry to VeroE6 cells (**Fig. S4**). Interestingly, alisol B 23-acetate revealed better antiviral effects on the Caco-2 cells than the A549-TMPRSS2 cells after exposed to *Omicron* BA5.2. challenge (Fig. 1**b and** Fig. 2**l**). Meanwhile, alisol B 23-acetate dose-dependently inhibited the invasion of *Omicron* S pseudotyped virions to HEK293-hACE2 cells (Fig. 3**d**). Alisol B 23-acetate also alleviated the interaction of ACE2 to the RBD of SARS-CoV-2 spike protein (Fig. 3**e**). The results of alisol B 23-acetate on virus attachment revealed the consistent effects that alisol B 23-acetate reduced the SARS-CoV-2 attachment to VeroE6 cells, dose-dependently (Fig. 3**f and 3g**). Those results suggest that the antiviral mechanisms of alisol B 23-acetate could be attributed to blocking the virus entry into cells via ACE2 rather than TMPRSS2.

We next conducted HDX-MS analysis to explore the potential reaction between ACE2 and alisol B 23-acetate. After deuterium exchange and digestion, the drug and protein mixture were analyzed by using high resolution MS. The sequence coverage to ACE2 (residues 18–740) was at 88.1 % (Fig. 3**h** and **Fig. S5**). Treatment of alisol B 23-acetate remarkably delayed the deuterium uptake of 7 peptide residues at 53–74, 134–167, 414–427, 497–511, 521–542, 553–567 and 569–585 (Fig. 3**i**), showing the HDX differences (ΔHDX) at −0.566 Da, −0.730 Da, −0.524 Da, −0.402 Da, −0.405 Da, −0.48 Da and −0.467 Da respectively in 60 min deuterium exchange. All these peptides impacted by alisol B 23-acetate were located at α-helical of ACE2 (Fig. 3**j**). Notably, the fragment covering residues 521–542, influenced by alisol B 23-acetate, was located at the helix (residues 511–531) which connected two subdomains and formed the floor of the canyon of ACE2 (Fig. S6**c**). We then performed molecular docking analysis to predict the binding activity of alisol B 23-acetate to ACE2. Consistently, the potential binding residues of alisol B 23-acetate were at P490, T497, G165 and L562 of ACE2 (Fig. 3**k and 3l**). These results indicate that alisol B 23-acetate inhibits coronavirus attachment to the cells through impacting activity of ACE2, subsequently blocking the virus entry and replication.

Alisol B 23-acetate reveals antiviral and anti-inflammatory properties in vivo

We then tested the antiviral properties of alisol B 23-acetate on the golden Syrian hamsters infected with SARS-CoV-2 and *Delta* variant *in vivo* using previous described protocol [38]. Similar to previous report [38], after exposed to SARS-CoV-2 or *Delta* variant at 3–4 days, the hamster lung tissues had the peak levels of viral loads with histopathological changes. In the study, alisol B 23-acetate (60 mg/kg) was intraperitoneally administrated to the hamsters for 3 days whereas the solvent injection was used as vehicle treatment. As shown in Fig. 4**a,** alisol B 23-acetate markedly reduced viral RNA level in the hamster lung tissues at ∼ 4-log10 and ∼ 15-log10 for SARS-CoV-2 and *Delta* variant, respectively (Fig. 4**b and 4f**). Meanwhile, alisol B 23-acetate significantly alleviated the SARS-CoV-2 and *Delta* variant plaque-forming units in the lung tissues by ∼ 1-log10 (Fig. 4**c and 4g**). Compared with the vehicle group, alisol B 23-acetate treatment significantly decreased the immunofluorescent staining of the viral N protein (VNP) in the lung sections with the infections of SARS-CoV-2 and *Delta* variant (Fig. 4**d-e** and Fig. 4**h-i**). Those results suggest that alisol B 23-acetate has anti-viral bioactivities against SARS-CoV-2 and *Delta* variant infection *in vivo.*

We also evaluated the pathogenesis of SARS-CoV-2 infection in lung tissues. After SARS-CoV-2 and *Delta* variant infection, hamster lung tissues had remarkably increased inflammatory cell infiltration around vascular endothelium areas and peribronchiolar regions that were characteristically companied with bronchus and alveoli tissue damages (Fig. 5**a and 5b**). The enlarged areas of bronchus and blood vessel indicated that bronchiolar epithelium cell death and perivascular infiltration were reduced after alisol B 23-acetate treatment. Thus, alisol B 23-acetate could be a promis-

Fig. 2. Alisol B 23-acetate (23-alisol B) has broad-spectrum inhibitive effects on human-pathogenic CoVs *in vitro*. Caco-2 cell line was infected with CoVs (multiplicity of infection (MOI) = 0.1) for 1 h and treated with 23-alisol B in 4 dosages (10, 20, 30, 40 μM) and remdesivir was used as positive control. (**a-f**) Virus titer in the cell culture supernatant were determined by plaque assay. After 1 h of infection and 24 h 23-alisol B treatment, viral titer of MERS-CoV (**a**) were determined. After 48 h 23-alisol B treatment, viral titer of SARS-CoVs-2 (**b**), *Alpha* variant (**c**), *Delta* variant (**d**), *Omicron* BA.1.1 variant (**e**), *Omicron* BA.5.2 variant (**f**) were detected in supernatant (n = 4 for each group, *p = 0.0233, **p = 0.0041 in MERS-CoV infection; **p = 0.0074 for 30 μM 23-alisol B, **p = 0.0019 for remdesivir in SARS-CoV-2 infection; **p = 0.0095 for 30 μM 23-alisol B, **p = 0.0031 for remdesivir in Alpha variant infection; *p = 0.0168 for 20 μM 23-alisol B in Delta variant infection; *p = 0.0314 for 10 μM 23-alisol B in Omicron BA.5.2 infection). (**g-l**) Intracellular viral loads were tested by qualitative polymerase chain reaction with reverse transcription and normalized by human β-actin. Relative inhibition rate of 23-alisol B was calculated by comparing viral loads in vehicle treated group. Relative inhibition of 23-alisol B on MERS-CoV (**g**) infection, SARS-CoVs-2 (**h**), *Alpha* variant (**i**), *Delta* variant (**j**), *Omicron* BA.1.1 variant (**k**) and *Omicron* BA.5.2 variant (**l**) (n = 3 for each group, **p = 0.0011 in MERS-CoV infection; **p = 0.0075 for Alpha variant infection; *p = 0.0468 for Delta variant infection). Viral titer and viral copies were normalized with cell viabilities or β-actin expression. All the data are presented as mean ± S.E.M (***p < 0.001, all comparations relative to vehicle group, one-way ANOVA followed by Dunnett test). All experiments were performed in n = 3–4 biological replicates and repeated twice for confirmation.

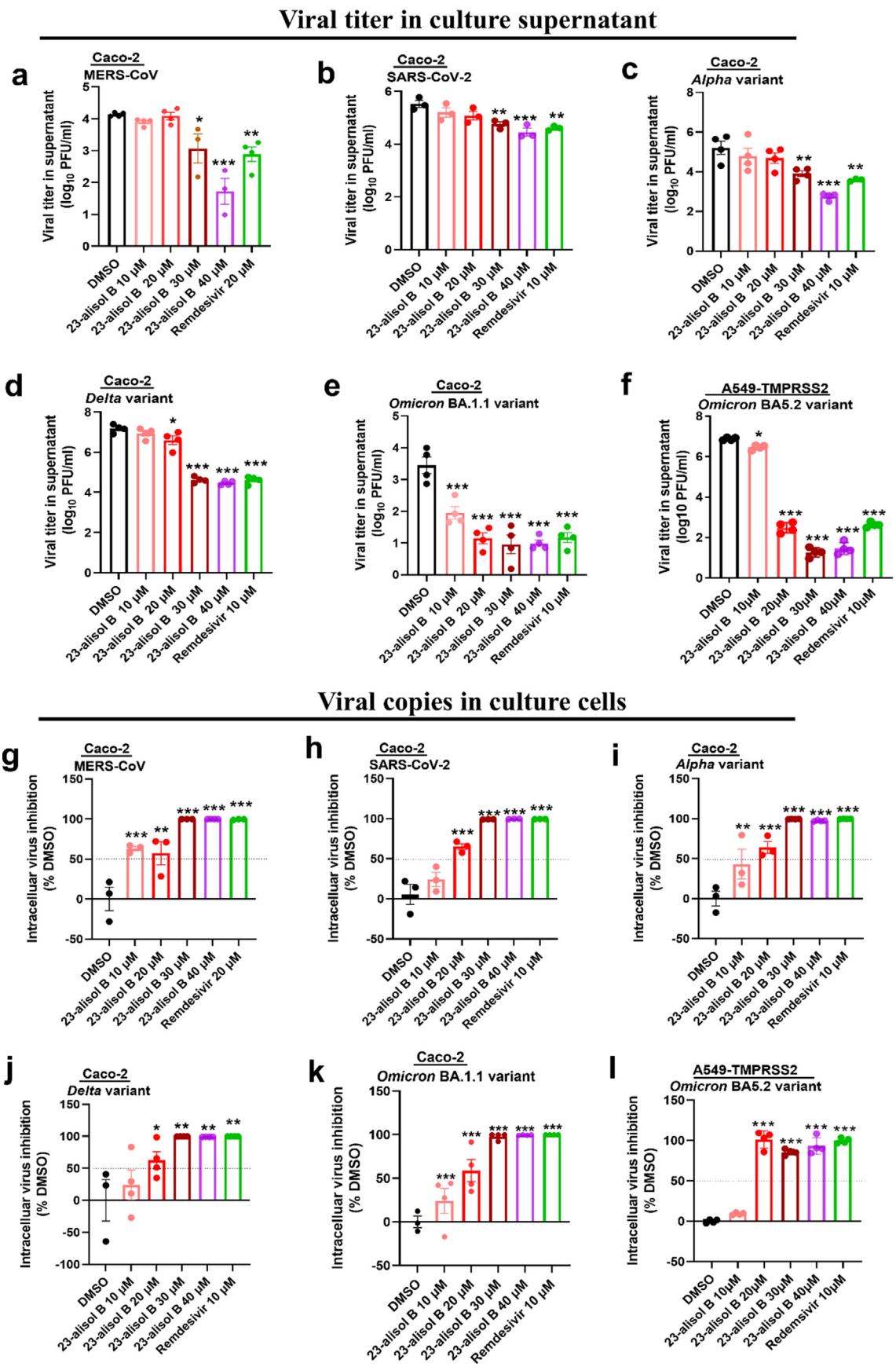
Viral titer in culture supernatant
a
Caco-2
MERS-CoV
Viral titer in supernatant (log10 PFU/ml)
b
Caco-2
SARS-CoV-2
c
Caco-2
Alpha variant
d
Caco-2
Delta variant
e
Caco-2
Omicron BA.1.1 variant
f
A549-TMPRSS2
Omicron BA5.2 variant
Viral titer in supernatant (log10 PFU/ml)
DMSO
23-alisol B 10 μM
23-alisol B 20 μM
23-alisol B 30 μM
23-alisol B 40 μM
Remdesivir 20 μM
Remdesivir 10 μM
Redemsivir 10μM
Viral copies in culture cells
g
Caco-2
MERS-CoV
Intracelluar virus inhibition (% DMSO)
h
Caco-2
SARS-CoV-2
i
Caco-2
Alpha variant
j
Caco-2
Delta variant
k
Caco-2
Omicron BA.1.1 variant
l
A549-TMPRSS2
Omicron BA5.2 variant

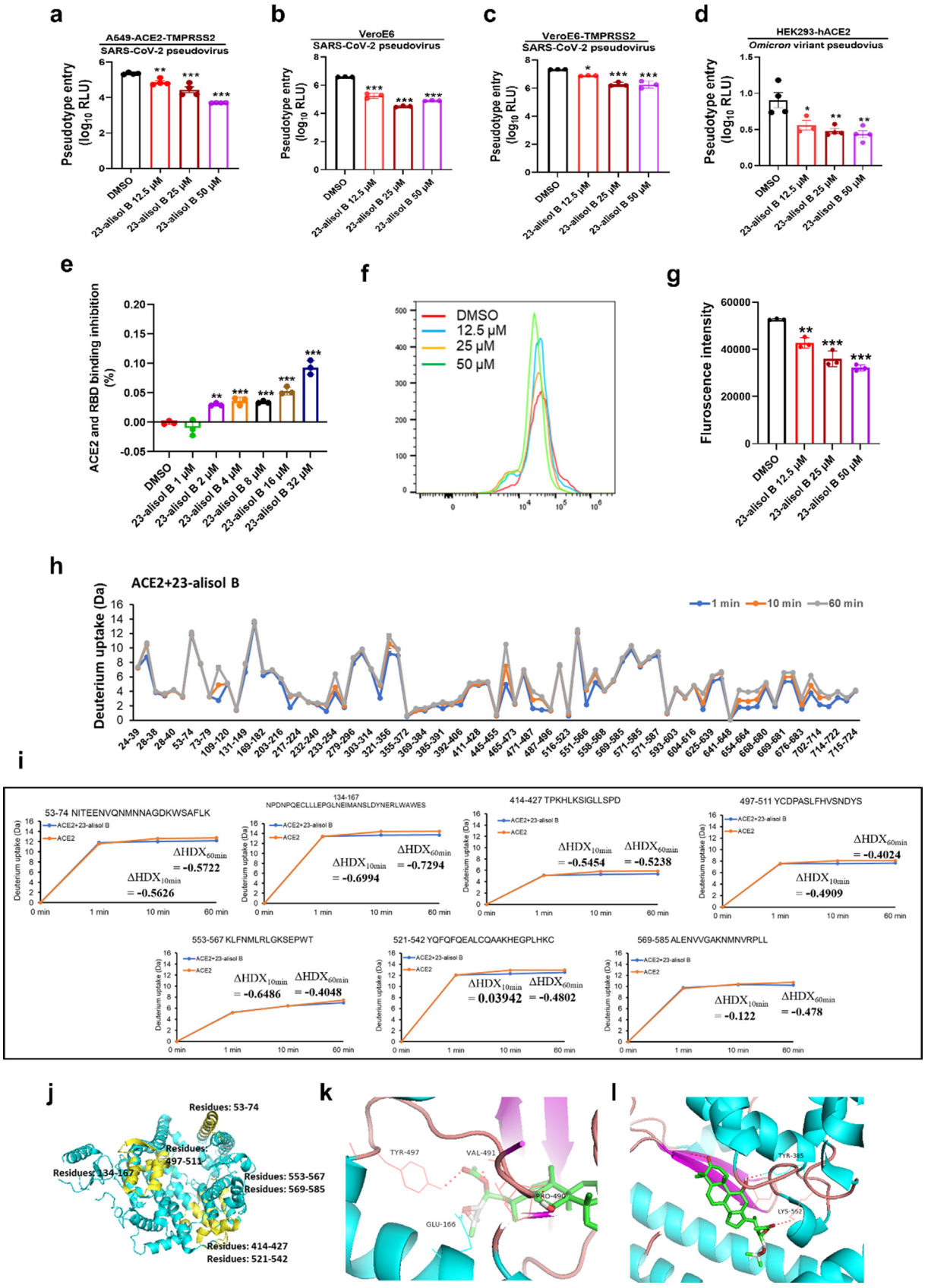

Fig. 3. Alisol B 23-acetate inhibits viral entry by targeting ACE2. (**a** - **c**) VSV-based pseudotyped viral particle of SARS-CoV-2 were pre-treated with 23-alisol B, and the relative mixture was added to targeted modified cells and kept in culture for 24 h. The SARS-CoV-2 pseudotype entry to A549-ACE2-TMPRSS2 cells (**a**), VeroE6 cells (**b**) and VeroE6-TMPRSS2 cells (**c**) were detected by the activity of firefly luciferase (n = 4, **p = 0.0081 for SARS-CoV-2 particles to A549-ACE2-TMPRSS2 cells; n = 3, *p = 0.0175 for SARS-CoV-2 particles to VeroE6 cells). (**d**) SARS-CoV-2 *Omicron* variant type pseudotyped viral particle entry was examined after incubation with 23-alisol B in HEK249-hACE2 cells (n = 4, *p = 0.0162, **p = 0.0024 for 25 μM 23-alisol B, **p = 0.0012 for 50 μM 23-alisol B). (**e**) ACE2 activity was detected through binding to RBD of wild type S protein by ELISA kit (n = 3, **p = 0.0014). (**f**) Representative flow cytometry histogram results of Spike protein related fluorescence intensity. (**g**) Quantification of spike protein intensity in VeroE6 cells (n = 3, **p = 0.0011). (**h**) Deuterium uptake of whole peptides of ACE2 after incubation with 23-alisol B. (**i**) Deuterium uptake results of significantly regulated peptides of ACE2 by 23-alisol B (n = 3 for each timepoint). (**j**) The location of impacted peptides were labeled onto the crystal model of ACE2. (**k** and **l**) Two potential binding sites of 23-alisol B to ACE2 and results shown as 3D molecular analysis. All the data are presented as mean ± S.E.M (***p < 0.001, all comparations relative to vehicle group, dunnett test, one-way ANOVA). All experiments were performed in n = 3–4 biological replicates and repeated twice for confirmation.

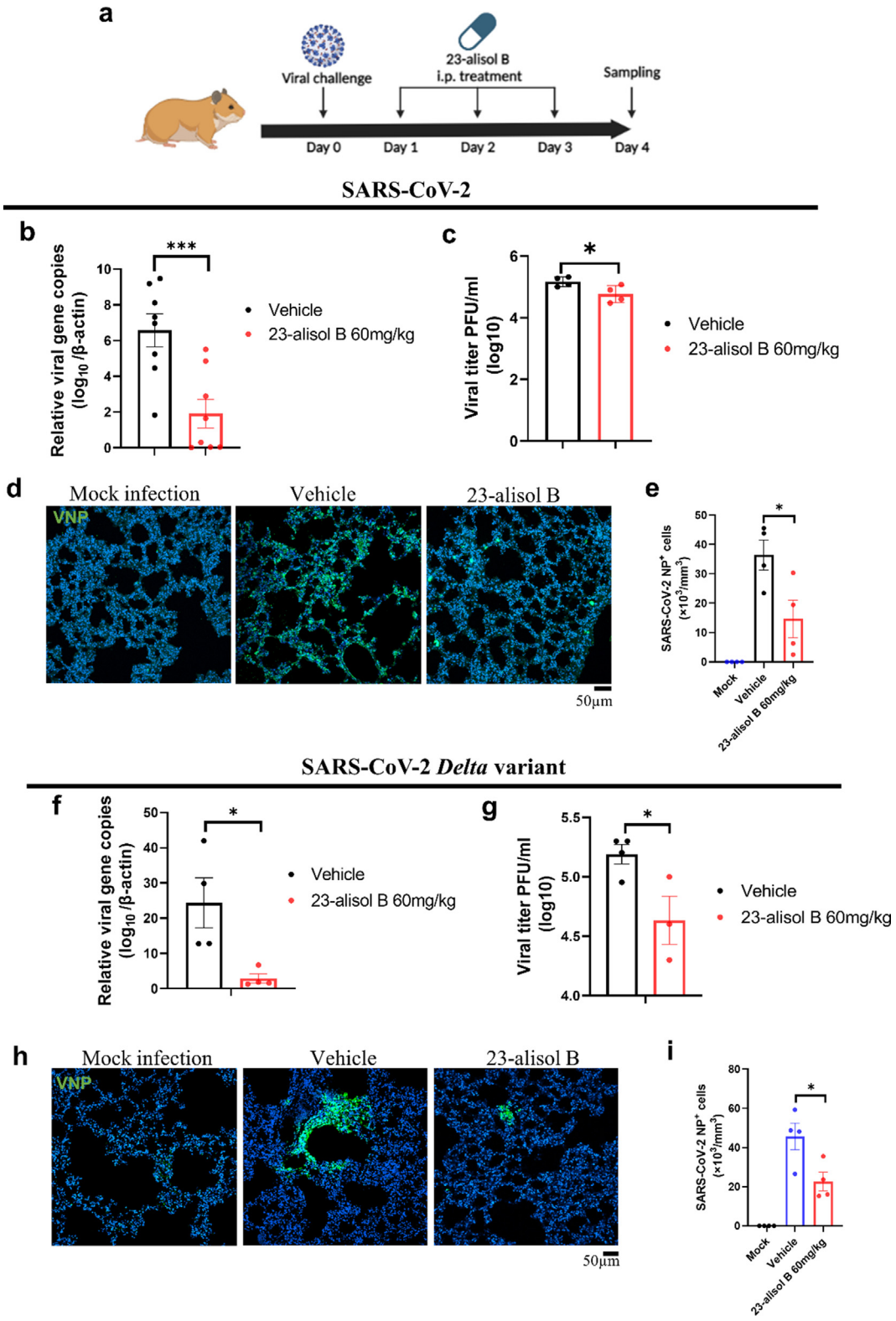

Fig. 4. Alisol B 23-acetate exhibits antiCoVs activities *in vivo*. (**a**) Hamsters (n = 4–8) were intranasally inoculated with 10^4 PFU of SARS-CoV-2 and SARS-CoV-2 *Delta* variant. Alisol B 23-acetate was intraperitoneal administration to hamster either vehicle (ethanol, PEG400 and saline solvent system) and 23-alisol B (60 mg/kg) for three consecutive days. (**b**) Virus copies in the hamster lung tissue after SARS-CoV-2 infection. Hamster lung collected at 3 dpi were subjected to SARS-CoV-2 viral copies detection by RT-qPCR assays (n = 8). (**c**) SARS-CoV-2 viral yield in the hamster lung tissue was titrated by plaque assays after 23-alisol B treatment for 3 days (*p = 0.0428). (**d**) Representative immunofluorescent images of the viral N protein (VNP) distribution in lung tissue sections after SARS-CoV-2 challenge. (**e**) Quantification of the cells positive with VNP colocalized with nucleus in SARS-CoV-2 challenged hamster lung tissue (*p = 0.0181). (**f**) Virus copies in the hamster lung tissue after *Delta* variant infection and 23-alisol B treatment (*p = 0.0249). (**g**) *Delta* variant viral yield in the hamster lung tissue (*p = 0.0359). (**h**) Representative immunofluorescent images of the VNP distribution in lung tissue sections after *Delta* variant challenge. (**i**) Quantification of the cells positive with VNP colocalized with nucleus in *Delta* variant challenged hamster lung tissue (*p = 0.0146). All the data are presented as mean ± S.E.M (***p < 0.001, all comparations relative to vehicle group, unpaired two-tailed Student's *t*-test between vehicle and 23-alisol B treatment group. One-way ANOVA was used for multiple groups designed experiments followed by Dunnett test for NP^+ cells. All experiments were performed in n = 4–8 biological replicates.

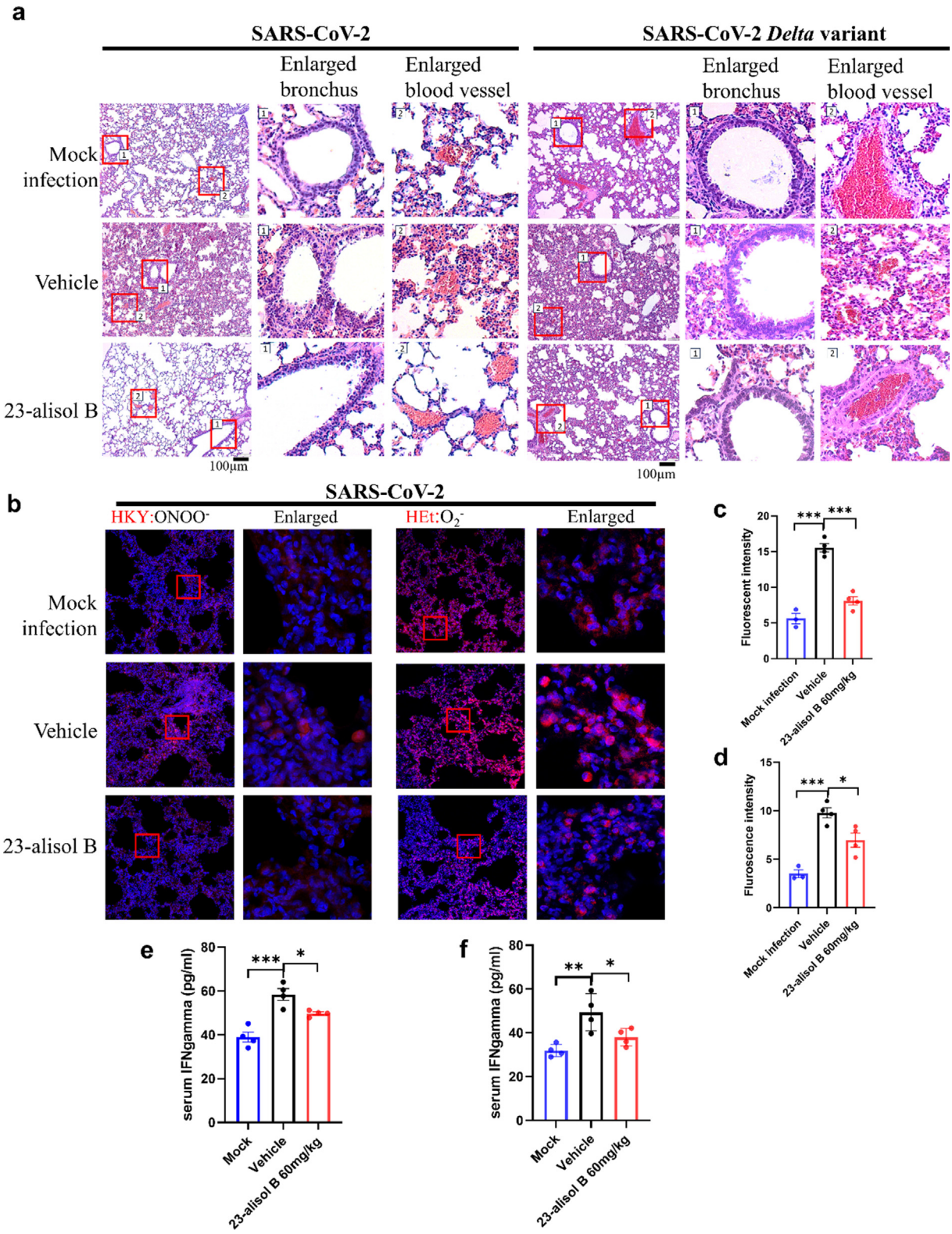

Fig. 5. Alisol B 23-acetate ameliorates lung damages in CoVs challenged hamster. Hamsters (n = 4–6) were intranasally inoculated with 10^4 PFU of SARS-CoV-2 and SARS-CoV-2 *Delta* variant. 23-alisol B was intraperitoneal administration to hamster either vehicle or 23-alisol B (60 mg/kg) for three consecutive days. (**a**) Representative images of H&E-stained lung tissue section from SARS-CoV-2 and *Delta* variant infected hamsters. Squared areas were shown as enlarged areas of bronchus and blood vessel. (**b**) Representative fluorescence micrographs of of HKYellow and hydroethidine (HEt) stained lung tissues of 23-alisol B and vehicle treated SARS-CoV-2 infected hamsters. (**c** and **d**) Quantification of HKyellow (**c**) and HEt (**d,** *p = 0.0167) fluorescence intensity in lung tissues. (**e-f**) Serum IFN-γ level in SARS-CoV-2 (**e**) and *Delta* variant (**f**) infected hamster serum were quantified by ELISA assay (*p = 0.0287 for IFNγ in SARS-CoV-2 infection; *p = 0.0339, **p = 0.0033 for *Delta* variant infection). All the data are presented as mean ± S.E.M (***p < 0.001, all comparations relative to vehicle group). All experiments were performed in n = 4–6 biological replicates.

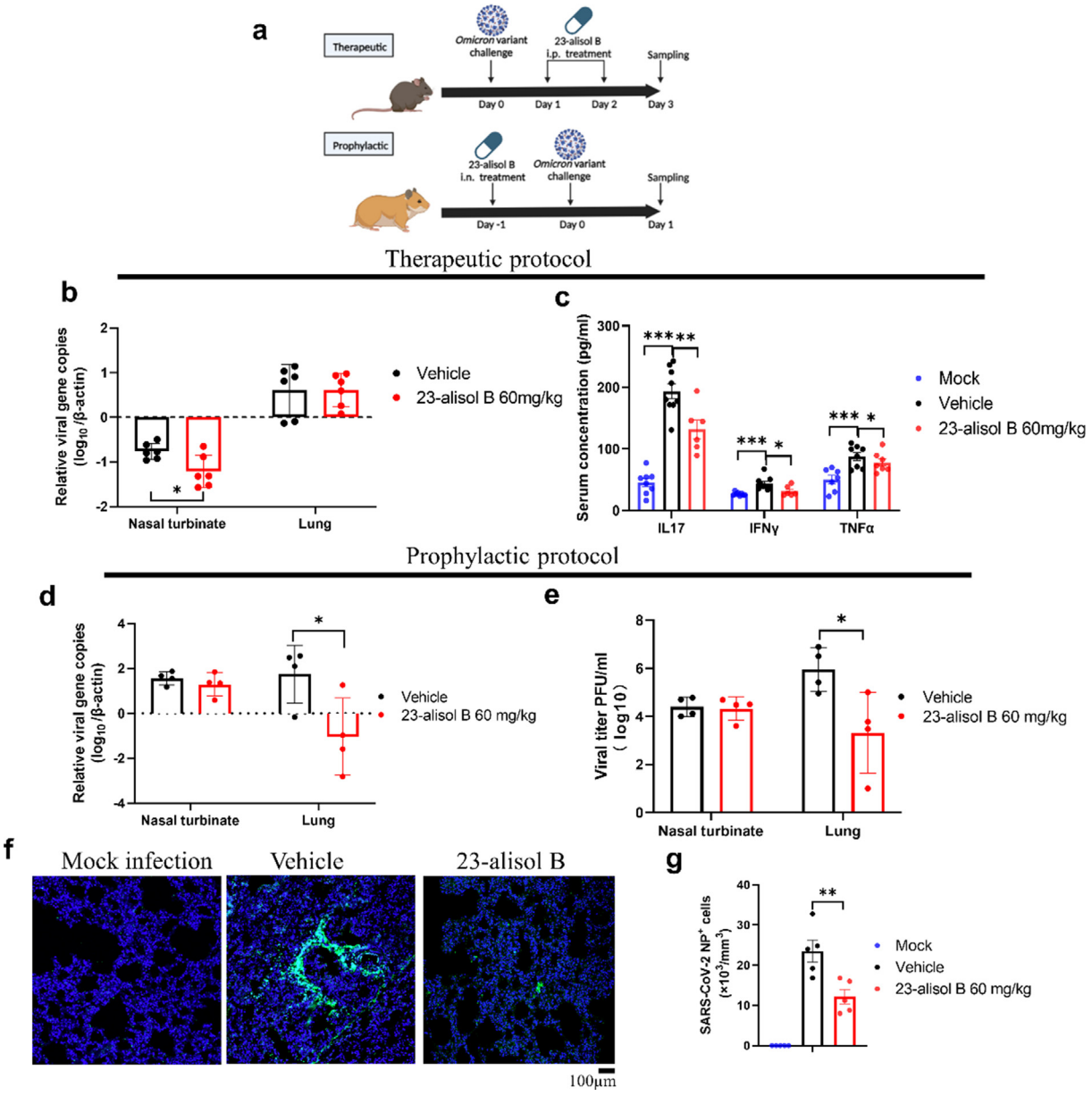

Fig. 6. Therapeutic and prophylactic treatment of 23-alisol B to *Omicron* variant infection in transgenic hACE2 mice and hamster. (**a**) hACE2 transgenic mice (n = 6–8) were intranasally inoculated with 10^5 PFU of SARS-CoV-2 Omicron variant and Omicron variant. For therapeutic effects, 23-alisol B was intraperitoneal administration to hamster either vehicle or 23-alisol B (60 mg/kg) for two consecutive days. Hamsters (n = 4–6) were intranasally inoculated with 10^5 PFU of SARS-CoV-2 *Omicron* variant. For prophylactic efficiency, 23-alisol B was intranasal administration to hamster with the same solvent system for one day before infection. (**b**) Virus copies in nasal turbinate and lung tissues of *Omicron* variant infected hACE2-mice (*p = 0.0224). (**c**) Inflammation cytokines detected by ELISA in serum of *Omicron* infected mice (*p = 0.018 for IFNγ content, *p = 0.0366 for TNFα content, **p = 0.003). (**d**) Viral yield was titrated by plaque assays in nasal turbinate and lung of hamster after viral infection (*p = 0.0410). (**e**) Viral copies in nasal turbinate and lung were detected by RT-qPCR assay (*p = 0.0426). (**f**) Representative immunofluorescence images of the viral N protein distribution in lung tissue sections. (**g**) Quantification of the cells positive with VNP colocalized with nucleus (**p = 0.0022). All the data are presented as mean ± S.E.M (***p < 0.001, all comparations relative to vehicle group, unpaired two-tailed Student's *t*-test between vehicle and 23-alisol B treatment group. one-way ANOVA followed by Dunnett test for NP^+ cells). All experiments were performed in n = 4–6 biological replicates.

ing natural compound with antiviral and anti-inflammatory bioactivities. Reactive nitrogen species (RNS) and reactive oxygen species (ROS) are important mediators for acute inflammatory responses and immune responses in acute respiratory distress diseases [47,48] as well as COVID-19 [49]. By using fluorescent probes hydroethiidine (HEt) and HKYellow (HKY), we detected the productions of superoxide and peroxynitrite in the hamster lung tissues respectively. The treatment of alisol B 23-acetate remarkably decreased the levels of superoxide and peroxynitrite in the lung tissues after SARS-CoV-2 and *Delta* variant infection (Fig. 5**c-5f**). In addition, SARS-CoV-2 and *Delta* variant infections significantly increased serum IFNγ level in the hamsters. While, alisol B 23-acetate treatment remarkably reduced serum IFNγ level in either SARS-CoV-2 or *Delta* variant infected hamsters **(**Fig. 5**g and 5h**). Those results suggest that alisol B 23-acetate ameliorates the cytokine storm and lung inflammatory damages induced by SARS-CoV-2 and *Delta* variant infection.

We further adopted hACE2-K18 mice and hamsters to study prophylactic and therapeutic effectiveness of alisol B 23-acetate against *Omicron* variant infection (Fig. 6**a**). Under the therapeutic protocol, alisol B 23-acetate treatment (i.p.) effectively attenuated viral copies in nasal turbinate by ∼ 0.5-log10 (Fig. 6**b**), but no statistical change of viral replications between vehicle and alisol B 23-acetate group was found in the *Omicron* variant infected lung tis-

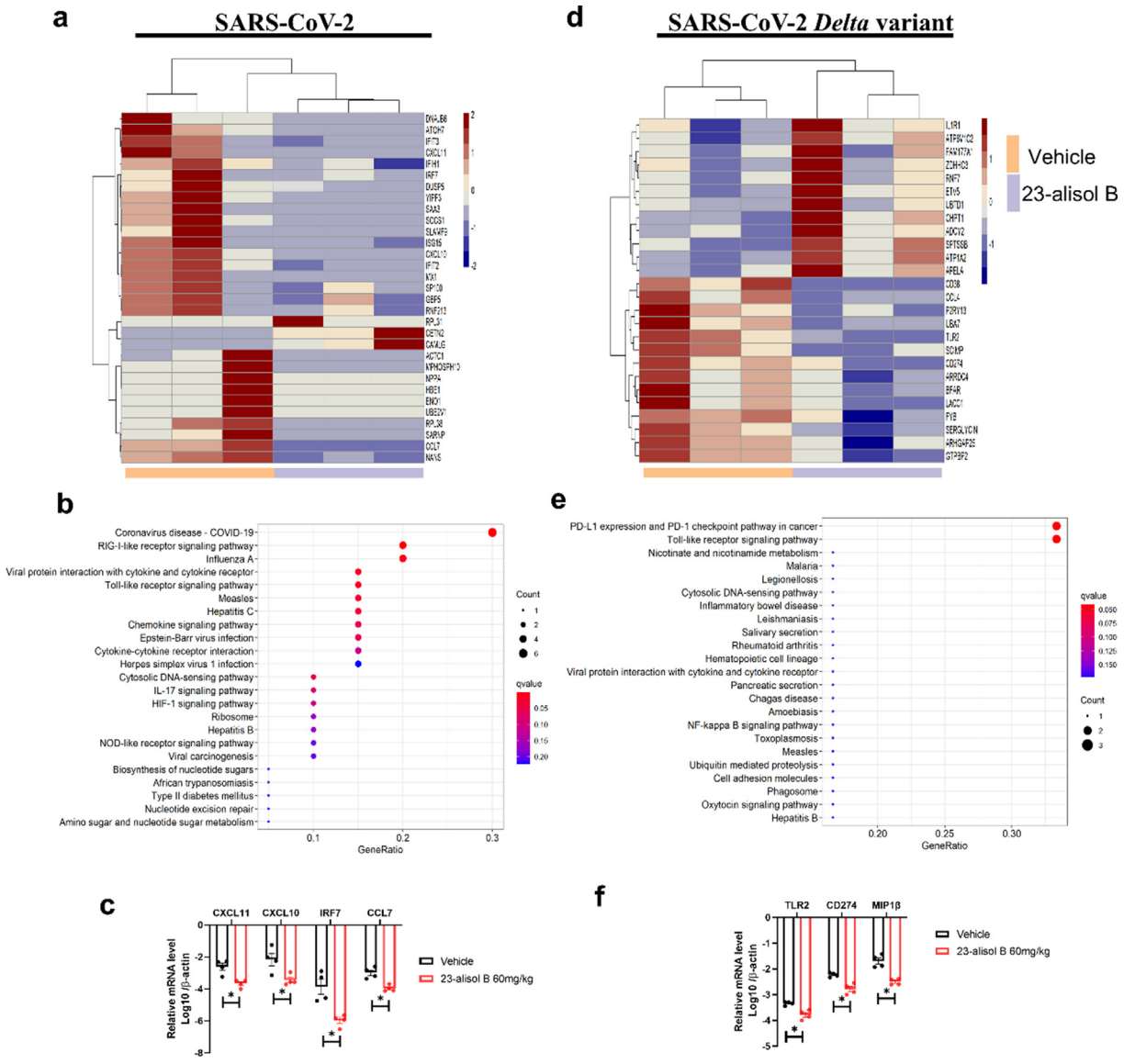

Fig. 7. Transcriptional analysis of SARS-CoV-2 and SARS-CoV-2 *Delta* variant infected hamster lung tissues with 23-alisol B treatment. (**a** and **d**) Heat map of DEGs in uninfected and SARS-CoV-2 (**a**) and *Delta* variant (**d**) infected hamster lungs administrated with therapeutic 23-alisol B or vehicle controls. (**b** and **e**) Pathway functional enrichment analysis results of down-regulated DEGs comparing 23-alisol B administration with its corresponding vehicle controls in SARS-CoV-2 (**b**) and *Delta* variant (**e**) infected hamster. (**c** and **f**) Representative expression level of chemokine and cytokine in the lung tissues homogenate from SARS-CoV-2 infection (**c**) and *Delta* variant (**f**) infection (n = 3–4) at 3 d.p.i. were detected by qRT-PCR assay (*p = 0.0296 for CXCL11, *p = 0.05 for CXCL10, *p = 0.0374 for IRF7, *p = 0.0291 for CCL7,*p = 0.0291 for TLR2, *p = 0.0157 for CD274, *p = 0.0211 for MIP1β). All the data are presented as mean ± S.E.M (All comparations relative to vehicle group, unpaired two-tailed Student's *t*-test between vehicle and 23-alisol B treatment group for mRNA expression levels).

sues. Additionally, alisol B 23-acetate treatment decreased IL17 and IFN-γ in the serum of *Omicron* variant infection, indicating the inhibition of proinflammatory cytokines (Fig. 6**c**). We then evaluated the prophylactic effects of alisol B 23-acetate against *Omicron* variant infection by using intranasal administration (i.n.) at 1-day before *Omicron* variant infection. Pre-treatment of alisol B 23-acetate significantly alleviated viral titer, viral loads and decreased viral N proteins in the hamster lung tissues (Fig. 6**d, 6e, 6f and 6g**). Those results support the potentials of alisol B 23-acetate as a promising drug candidate for COVID-19 treatment with the bioactivities of antiviral and anti-inflammation *in vivo*.

Transcriptional analysis of lung tissue treated with alisol B 23-acetate

We next performed RNAseq experiments to profile overall transcriptome changes in hamster lung tissues under SARS-CoV-2 or *Delta* variant infection. Alisol B 23-acetate treatment significantly down-regulated 28 genes and up-regulated 3 genes in the hamster lung tissues of SARS-CoV-2 infection (Fig. 7**a**). In the differential expression genes (DEGs) analysis for KEGG functional pathway, alisol B 23-acetate revealed to decrease the SARS-CoV-2 associated pathogenesis and proinflammatory signaling pathways, including IL17 signaling pathway, toll like receptor (TLR) signaling pathway and NOD-like receptor signaling pathway (Fig. 7**b**). Meanwhile, similar effects were found in the samples with *Delta* variant infection. At 4 dpi, alisol B 23-acetate treatment affected 26 genes in the *Delta* variant infected hamsters (Fig. 7**d**). Among them, alisol B 23-acetate down-regulated TLR signaling pathway in both WT type and *Delta* variant infection (Fig. 7**b and 7e**). Furthermore, alisol B 23-acetate treatment significantly downregulated the mRNA expression of CXCL10, CXCL11, CCL7 and IRF7 in the SARS-CoV-2 infected hamster lung tissues (Fig. 7**c**). Alisol B 23-acetate also suppressed the expression levels of TLR2 and MIP1β in the *Delta* infected hamster lung tissues (Fig. 7**f**). Those results indicate that

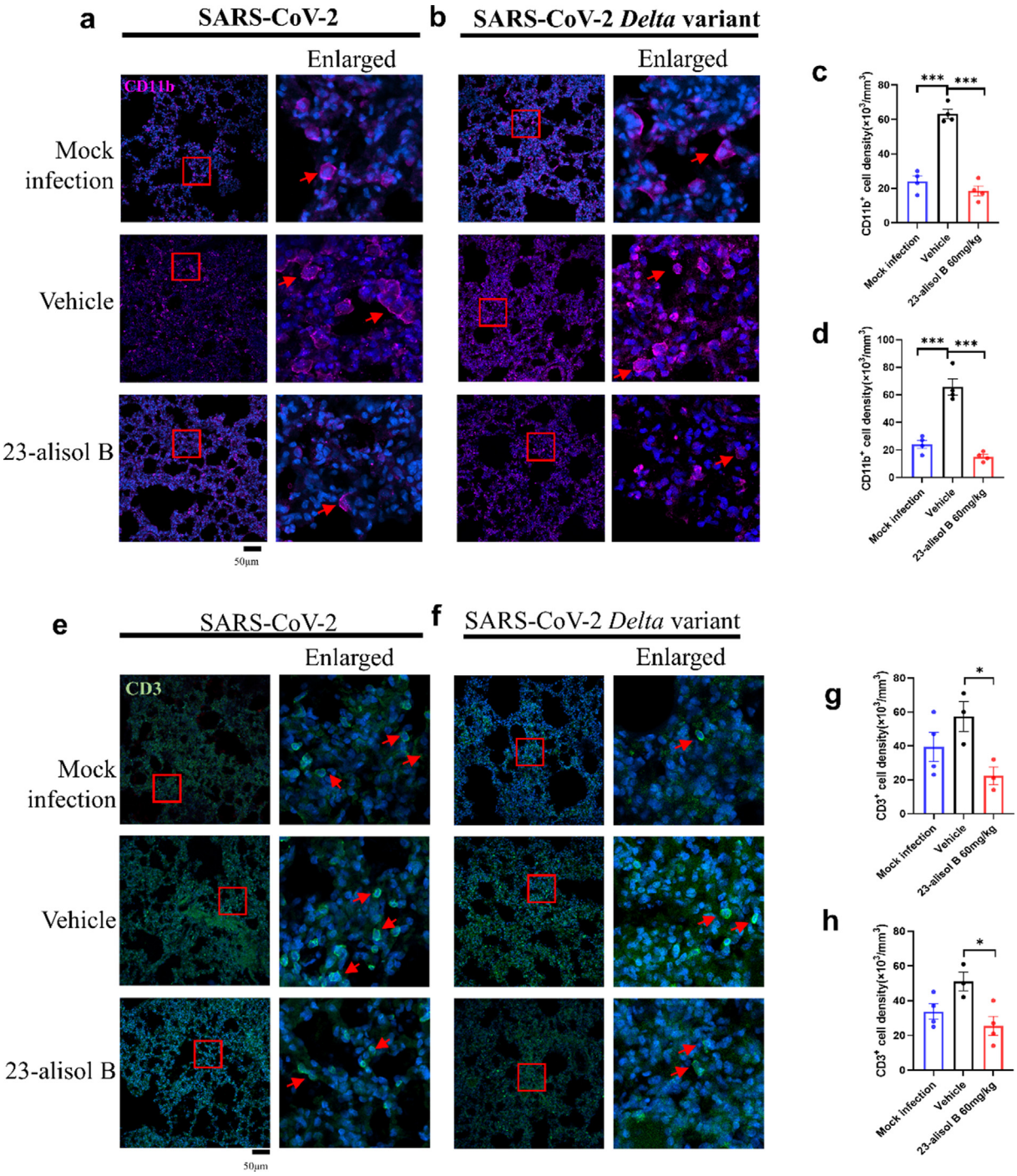

Fig. 8. Alisol B 23-acetate decreases macrophages and T cells infiltration in lung tissues of SARS-CoV-2 and *Delta* variant infection. (**a** and **c**) Representative confocal images of the CD11b positive macrophages in lung tissue sections after SARS-CoV-2 (**a**) infection and SARS-CoV-2 *Delta* variant (**c**) infection. (**b** and **d**) Quantification of the density of CD11b positive cells in lung tissues of SARS-CoV-2 (**b**) and SARS-CoV-2 *Delta* variant (**d**) infection. (**e** and **g**) Representative confocal images of the CD3 positive T lymphocytes in lung tissue sections after SARS-CoV-2 (**e**) infection and SARS-CoV-2 *Delta* variant (**g**) infection. (**f** and **h**) Quantification of the density of CD3 positive cells in lung tissue sections after SARS-CoV-2 (**f**) infection and SARS-CoV-2 *Delta* variant (**h**) infection. All the data are presented as mean ± S.E.M (***p < 0.001, all comparations relative to vehicle group, Dunnett test, one-way ANOVA). All the quantification were conducted based on 2 views in one sample.

alisol B 23-acetate could modulate the inflammatory response related signal pathways in SARS-CoV-2 or *Delta* variant infection.

Alisol B 23-acetate suppress proinflammatory T cells responses

Macrophages and T cells play crucial roles in mediating cytokine storm in severe COVID-19 patients [50,51]. Our RNAseq experiments suggest the inhibitory effects of alisol B 23-acetate on TLR related proinflammatory responses. Thus, we further investigated the effects of aliso B on $CD11b^+$ macrophages and $CD3^+$ T cells in the virus infected hamsters. Administration of alisol B 23-acetate tremendously reduced the numbers of $CD11b^+$ macrophages (Fig. 8**a-8d**) and $CD3^+$ T cells infiltration (Fig. 8**e-8h**) in the hamster lung tissues. Since aliso B 23-acetate could directly inhibit viral entry into cells, one may argue that the inhibitions of the macrophages and T cell infiltration could be attributed to

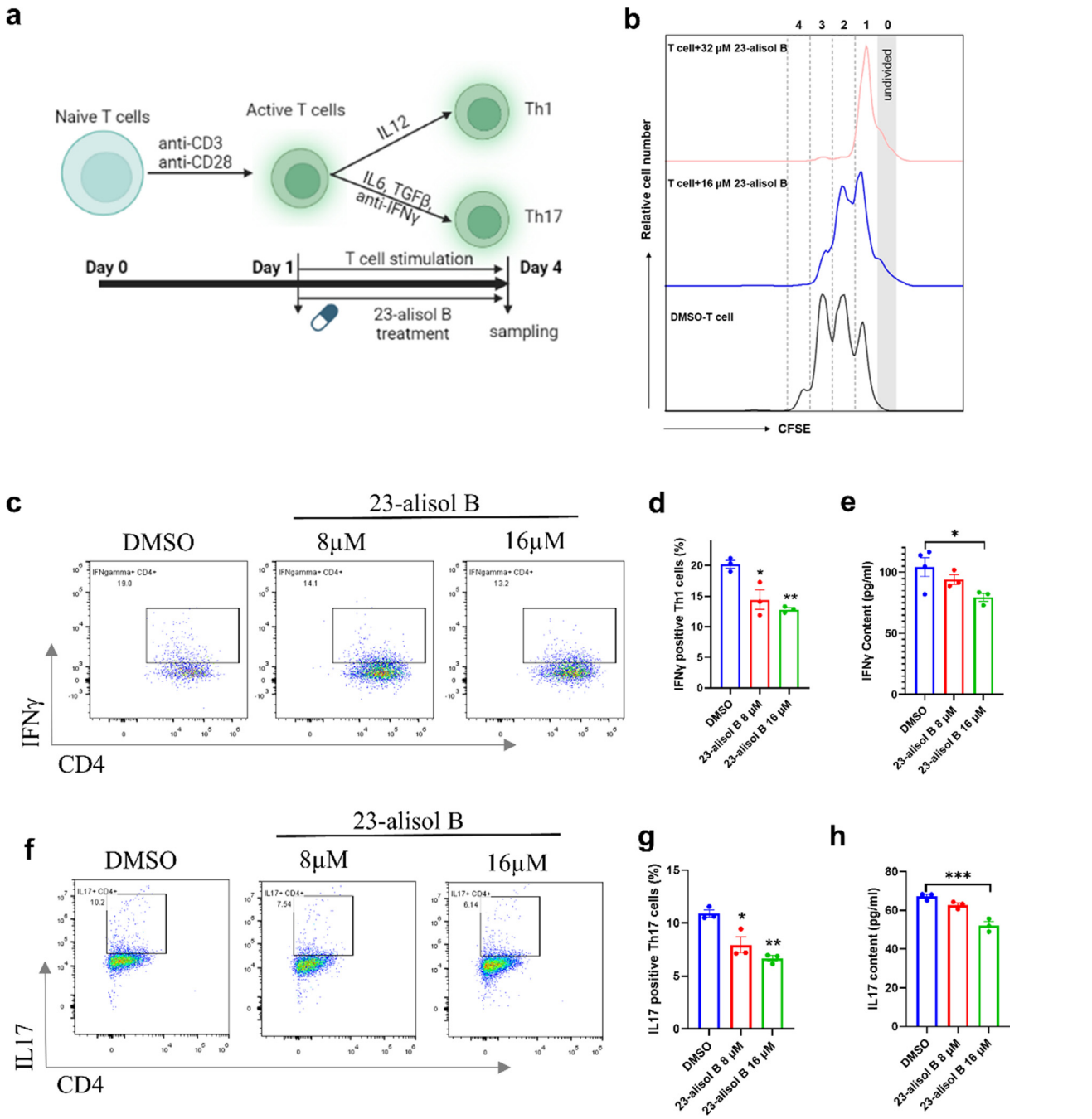

Fig. 9. Alisol B 23-acetate suppressed pro-inflammatory T cells activation and cytokines release in human lymphocytes *in vitro*. (**a**) T cells stimulation and 23-alisol B treatment procedure. Anti-CD3 and anti-CD28 antibody were pre-coated for the activation and expansion of human T cells. Alisol B 23-acetate was treated to the activated T cells for 72 h before analysis. (**b**) The proliferation of $CD4^+$ T cells was evaluated by CFSE detection through flow cytometry. (**c** and **f**) Representative flow cytometry results of $IFN\gamma^+$ T cells (**c**) and $IL17^+$ T cells (**f**) treated with 23-alisol B and DMSO as control. (**d** and **g**) Quantification of the percentage of $IFN\gamma^+$ T cells (**d**) and $IL17^+$ T cells (**g**) positive cells in 23-alisol B treated T cells (*p = 0.0112, **p = 0.0035 for Th1 cells population, *p = 0.0447 for IFNγ content). (**e** and **h**) The content of IFNγ (**e**) and IL-17 (**h**) was assessment in cell culture supernatant after 48 h treatment (*p = 0.0103, **p = 0.0018). All the data are presented as mean ± S.E.M (***p < 0.001, all comparations relative to vehicle group, Dunnett test, one-way ANOVA). All experiments were performed in triplicate and repeated twice for confirmation.

the reduction of the viral loads in the targeted tissues. Thus, we investigated the activities of alisol B 23-acetate on pro-inflammatory T cells *in vitro* to confirming the direct anti-inflammatory and immunomodulation activities by adopting primary mouse immune cells and human PBMC *in vitro*. To mimic the proinflammatory T cells activation in viral infection, we induced T helper 1 (Th1) cells and T helper 17 (Th17) cells by using several cytokines (Fig. 9**a**). We used CD4 related isotype control to get the CD4 positive population (**Fig. S7**). CFSE labeling was applied to study the role of alisol B 23-acetate on T cells proliferation. Alisol B 23-acetate treatment significantly inhibited the proliferation of T cells (Fig. 9**b**) and decreased the differentiation of T cells into Th1 cells with the lower population of $IFN\gamma^+CD4^+$ cells (Fig. 9**c and 9d**). The secretion of IFNγ was also decreased in the supernatant (Fig. 9**e**). Furthermore, we observed the roles of alisol B 23-acetate on proinflammatory Th17 cells and IL17 secretion. Treatment of alisol B 23-acetate for 48 h inhibited the population of the $IL17^+CD4^+$ dual positive Th17 cells (Fig. 9**f and 9g**) and attenu-

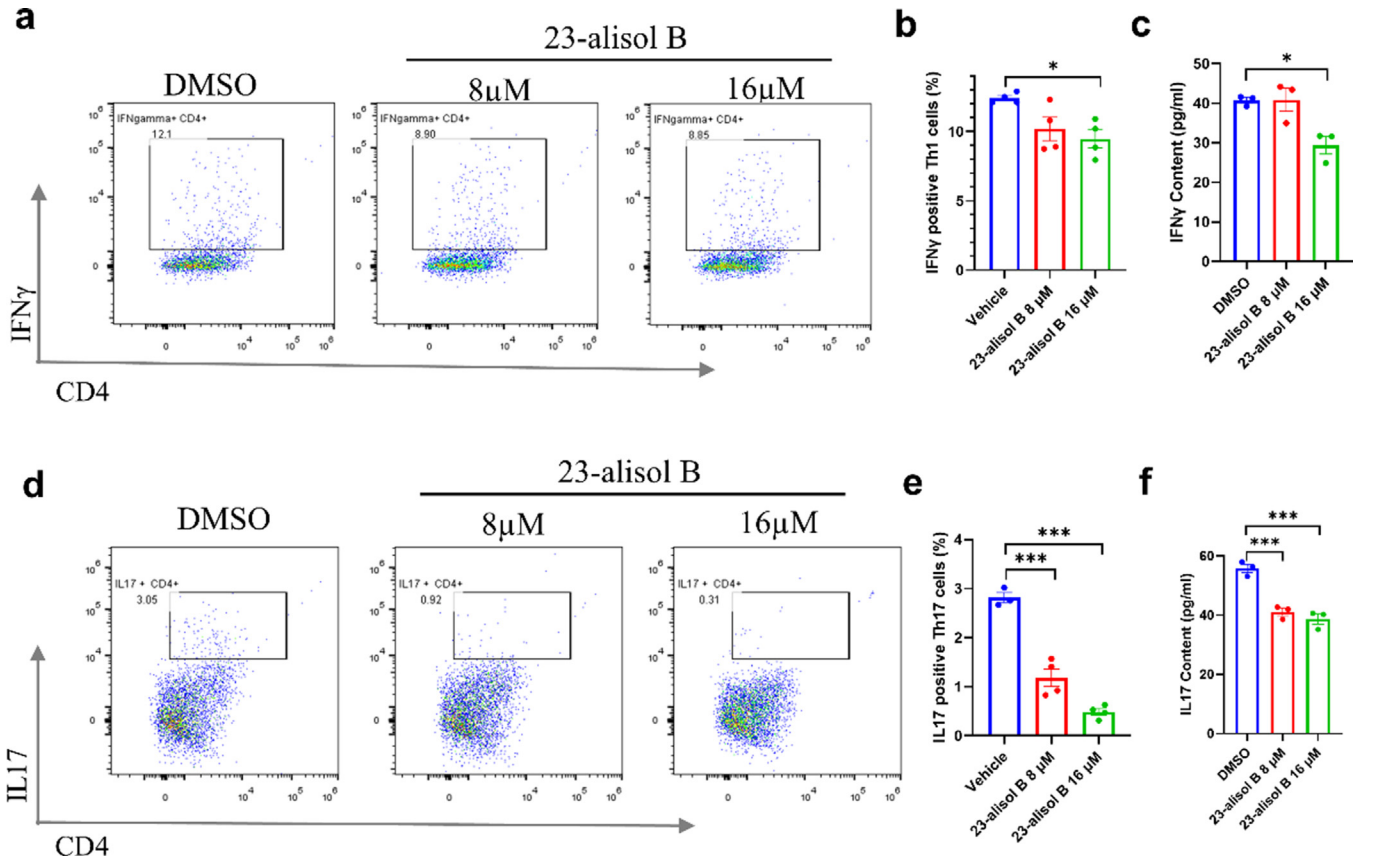

Fig. 10. Alisol B 23-acetate suppressed pro-inflammatory T cells activation and cytokines release in mice lymphocytes. (**a** and **d**) Representative flow cytometry results of IFNγ$^+$ T cells (**a**) and IL17 $^+$ T cells (**d**) treated with 23-alisol B and DMSO as control. (**b** and **e**) Quantification of the percentage of IFNγ$^+$ T cells (**b**) and IL17 $^+$ T cells (**e**) positive cells in 23-alisol B treated T cells (*p = 0.0171). (**c** and **f**) The content of IFNγ(**c**) and IL-17 (**f**) was assessment in cell culture supernatant after 48 h treatment (*p = 0.0154). All the data are presented as mean ± S.E.M (***p < 0.001, all comparations relative to vehicle group, Dunnett test, one-way ANOVA). All experiments were performed in triplicate and repeated twice for confirmation.

ated the release of IL17 into the culture supernatant (Fig. 9**h**). Similarly, in primary cultured mouse lymphocytes, alisol B 23-acetate decreased the population of the IFNγ positive Th1 cells and attenuated IFNγ secretion (Fig. 10**a-10c**). As for Th17 cells, alisol B 23-acetate showed the suppressive effects on IL17 concentration and IL17$^+$ Th17 cells (Fig. 10**d-10f**). Finally, we measured the population of T follicular helper (Tfh) cells but no remarkable change was found in the iCOS$^+$ and PD1$^+$ Tfh cells population after alisol B 23-acetate treatment (Fig. S8**a and S8b**). Overall, these results suggest that alisol B 23-acetate could inhibit proinflammatory T lymphocyte responses.

Discussion

In the present study, we firstly screened 35 active compounds identified from QFPD with the potentials of antiviral bioactivities. Among them, alisol B 23-acetate was the only compound with the inhibitory effects on SARS-CoV-2 infection *in vitro*. Further studies revealed that alisol B 23-acetate had broad inhibitory effects on different coronavirus species including MERS-CoV, SARS-CoV-2, SARS-CoV-2 *Alpha* variant, *Delta* variant and *Omicron* variant *in vitro* and *in vivo*. HDX-MS study indicates that the potential binding sites of alisol B 23-acetate could be at spike protein receptor ACE2. Moreover, a series of *in vivo* and *in vitro* experiments suggest that alisol B 23-acetate could inhibit proinflammatory T cells responses and ameliorate the CoVs infection-induced inflammation.

Alisol B 23-acetate is presented in *Alismatis Rhizoma*, a medicinal plant from GFPD. Given that alisol A/B/C and their acetates are structurally similar compounds identified from *Alismatis Rhizoma,* we subsequently investigated the structure and functional relationship for their anti-coronavirus bioactivities. Notably, both alisol B and alisol B 23-acetate dose-dependently reduced the viral load in the supernatant of the *Omicron* infected Caco-2 cells. Although alisol A/alisol A 24-acetate and alisol C/alisol C 23-acetate are structurally similar to alisol B or alisol B 23-acetate, all of them had no inhibitory effect on the viral load. The major structural differences among those compounds are the acetoxy group and carbonyl group. Particular attention could be paid to the structural difference between alisol B 23-acetate and alisol C 23-acetate. The carbonyl group of alisol C 23-acetate could make the rotatable structural changes that might affect its antiviral bioactivity (Fig. 1). While, the acetoxy group of alisol B 23-acetate could form a polar connect to residue 497, a special binding site of S-protein in ACE2 (Fig. 3**j**). Whether the acetoxy group and carbonyl group are essential groups for antiviral bioactivities of alisol compounds remains to be elucidated.

ACE2 is a major receptor protein mediating SARS-CoV-2 entry to the host cells [41,52]. The structure arrangement in the spike protein S2 subunit impacts the fusion of SARS-CoV-2 with host cell membranes [53,54]. The *Omicron* spike protein exhibits the strengthened S-ACE2 interaction and high ACE2 affinity to form S-ACE2 complex, facilitating the transmissibility and immune evasion [55]. Herein, we found that alisol B 23-acetate blocked the entry of SARS-CoV-2 S pseudotyped virions into VeroE6 cells, A549-ACE2-TMPRSS2 cells and VeroE6-TMPRSS2 cells. It also diminished the *Omicron* variant S pseudotyped virions entry into HEK293-hACE2 cells. According to the crystal structure, ACE2 is

composed of 20 α-helical segments and nine 3_{10} helical segments in secondary structure [56,57] (Fig. S6**a**). Helix H1 (Q24-Q42), beta sheet (K353-R357) and helix H2 (L79-Y83) are the binding domains of ACE2 receptor to the Spike protein [58,59]. Additionally, several hydrogen bonds are formed in the interaction of ACE2 and SARS-CoV-2 RBD locating at residues N417, Y505, T500 and N501[59]. In HDX-MS analysis, alisol B 23-acetate acted on α-helical of ACE2 located at residues 53–74, residues 134–167, residues 414–427, residues 497–511, residues 521–542, residues 553–567 and residues 569–585. The residues 521–542 at the helix (residues 511–531) could connect the subdomains to form the floor of the canyon of ACE2, whereas residues 53–74 are near to the binding region of ACE2 linking to the RBD. The peptide 53–74 affects the conformational change of ACE2 induced by the neighborhood. Alisol B 23-acetate also affected several hydrogen bonds locating at residues N417, Y505, T500 and N501 that participate in the interactions between ACE2 and SARS-CoV-2 RBD [59]. Moreover, the acetoxy group could form a polar connect for alisol B 23-acetate to residue 497 in ACE2, subsequently affecting the flexibility of the ACE2 (Fig. 3**k** and **Fig. S9**). By using HDX-MS, we further analyzed 84 peptides in ACE2 protein that achieved 88.1 % coverage (Fig. 3**f** and **Fig. S4**). Unfortunately, we were unable to detect precursor ion (516.7, 517.7, 518.7 and 519.7 in positive charge model) of alisol B 23-acetate in any of these peptides. Alisol B 23-acetate dose-dependently block S-ACE2 complex (Fig. 3**e**). Thus, we expect that alisol B 23-acetate could bind to ACE2 non-covalently rather than directly ACE2-binding activity. The anti-coronavirus mechanism of alisol B 23-acetate could be, at least in part, attributed to blocking S-ACE2 interaction and preventing the virus entry into cells. Notably, ACE2 is essential for blood pressure regulation through ACE2/angiotensin-(1–7)/MAS-receptor (ACE2/ANG-(1–7)/MAS) axis [60]. Infection of SARS-CoV-2 led to reduce the expression of ACE2 and affect RAAS [61]. Alisol B 23-acetate could regulate gut-kidney axis and reduce blood pressure in rat models of hypertension and chronic kidney disease [62]. Whether alisol B 23-acetate affects blood pressure in COVID-19 treatment remains to be further studied.

Cellular serine protease TMPRSS2 is also an essential mediator for S protein priming [63–65]. However, alisol B 23-acetate showed lower antiviral bioactivities in A549-TMPRSS2 cells under the challenge of *Omicron* BA5.2. variant (Fig. 1**b and** Fig. 2**l**). Thus, TMPRSS2 might be not involved in the antiviral bioactivities of alisol B 23-acetate. Recently, neuropilin1 and furin are identified as co-factors for viral entry, especially in the cells with low ACE2 expression [66,67]. It is of interesting to address whether alisol B 23-acetate affects those co-factors in future.

Hamster and human ACE2 transgenic mice are two well established and widely used animal models for COVID-19 study [68,69]. With the sustained mutations in RBD region of SARS-CoV-2 spike protein, different types of variants are characterized with different transmissibility and pathogenicity. We adopted hamsters and hACE2 transgenic mice to evaluate the antiviral activities *in vivo*. Alisol B 23-acetate was intraperitoneally injected into hamsters for improving bioavailability. In both SARS-CoV-2 and *Delta* variant infected hamsters, treatment of alisol B 23-acetate significantly declined the viral copies and viral N protein expression in the lung tissues (Fig. 4) and ameliorated lung damages (Fig. 5). Those results suggest that alisol B 23-acetate could dampen SARS-CoV-2 and *Delta* variant infection and attenuate lung damages. In our previous study, *Omicron*-infected hamsters exhibited lesser respiratory tract viral burdens and lung damage than *Delta*-infected hamsters [45]. *Omicron* variant infection had lesser pulmonary changes than *Delta* infection in the computed tomography imaging of COVID-19 patients [70]. Accordingly, we investigated the therapeutic and prophylactic effects of alisol B 23-acetate on the *Omicron* variant infection by detecting the viral copies in the nasal turbinate and lung tissues. The mice were received the treatments of alisol B 23-acetate or vehicle under anesthesia to reduce the pain and mucociliary clearance. Interestingly, in the therapeutic protocol, alisol B 23-acetate treatment intraperitoneally significantly attenuated viral copies in nasal turbinate. In the prophylactic intranasal administration, alisol B 23-acetate remarkably decreased the viral copies and the expression of VNP in the lung tissues but had no influence on the viral load of the nasal turbinate (Fig. 6). With the intranasal administration, we could minimize potential side effects of alisol B 23-acetate and make easy for the prevention and treatment of COVID-19. Therefore, alisol B 23-acetate could be a potential antiviral agent against SARS-CoV-2, *Delta* and *Omicron* variant infections.

Oxidative stress and inflammatory response are implicated as major causes of cytokine storm with high mortality in COVID-19 patients [71,72]. The macrophages and T cells aggravate inflammation cascade reactions, contributing to severe SARS-CoV-2 pneumonia [51,73]. IFNγ and IL17 are two proinflammatory cytokines correlated with lung injury in the critical illness patients [74–76]. Inflammatory factors and immune cytokines, including anti-IL17 and anti-IFNγ, are crucial therapeutic targets for COVID-19 treatment [77–79]. Th1 and Th17 cells are the major sources of IFNγ and IL17, respectively, and inhibition of those immune cells could reduce cytokines-mediated tissue damages [80]. Superoxide (O_2^-) and peroxynitrite ($ONOO^-$) are critical mediators contributing to lung damages in COVID-19 [49,81,82]. As a result, we investigated the antioxidant and anti-inflammation effects. Treatment of alisol B 23-acetate diminished the productions of O_2^- and $ONOO^-$ in the lung tissues and reduced serum IFNγ level in the SARS-CoV-2 and *Delta* variant infected hamsters. It also reduced serum concentrations of IL17, IFNγ and TNFα in the hACE2 transgenic mice with *Omicron* variant infection. Furthermore, alisol B 23-acetate inhibited the infiltration of T cells and macrophages in the hamster lung tissues. Consistent results were also observed from *in vitro* experiments. Alisol B 23-acetate reduced the secretion of IL17 and IFNγ in normal lymphocyte activation, suggesting the anti-inflammatory effects and suppression of cytokine storm in viral infection. By using transcriptional analysis, our study indicates that alisol B 23-acetate could modulate the inflammation response related signal pathways. Notably, ACE2 is not presented in T cells [83–86]. CD26 and CD147 play vital roles in SARS-CoV-2 infection of T cells [83,87,88]. Although alisol B 23-acetate could bind to ACE2, its effects on pro-inflammatory T cells should be ACE2-independent. Taken together, alisol B 23-acetate could inhibit oxidative stress and cytokine storm in the animals with the SARS-CoV-2, *Delta* or *Omicron* variant infection.

Cytotoxicity is an important topic for drug discovery. In the *in vitro* results, the highest SI value of alisol B 23-acetate was 4.16. Alisol B 23-acete showed potential cytotoxicity with CC50 ranged from 22 to 46 μM *in vitro* (Fig. 1**c** and **Fig. S2**). Hence, we performed acute toxicity experiments in which the hamsters were treated with alisol B 23-acetate at 360 mg/kg, a six-time higher dosage than the therapeutic one used in our study. The treatment had no influence on body weight, organ functions, liver functions and tissue morphological change. Previous pharmacokinetic study revealed that alisol B 23-acetate had the half-life time at 8.43 h in rat plasma [89]. Also, alisol B 23-acetate treatment at 60 mg/kg for 4 weeks had non-cytotoxic effects on non-alcoholic steatohepatitis mice *in vivo* [90]. Taken together, alisol B 23-acetate should be safe as an antiviral agent. For drug discovery, the long-term safety, pharmacodynamical profiles and metabolic kinetics remain to be further explored.

Last but not least, we should note the limitation of this study. Firstly, for fast-track drug screening to fight COVID-19 timely, we

only selected 35 compounds from QFPD, a commonly used TCM formula in Chinese community. Of the potential active compounds, alisol B 23-acetate may not be the best anti-coronavirus compound in the formula. Plus, the concentration and bioavailability of alisol B 23-acetate in QFPD are unknown yet. We should be cautious to use the experimental results for the interpretation of the QFPD's anti-COVID-19 mechanisms and chemical basis. Next, we only preformed the acute toxicity studies on alisol B 23-acetate. With potential cytotoxicity *in vitro*, for drug discovery, we would modify the structures for better bioavailability and less toxicity. Pharmacokinetics, pharmacodynamics and comprehensive toxicity studies shall be performed before clinical trials. Furthermore, the pharmaceutical investigations, such as nasal spray development or sustained-release preparations, are important to achieve satisfied results in translational application of alisol B 23-acetate.

Conclusions

Alisol B 23-acetate is a valuable medicinal compound with anti-pan-CoVs bioactivities for COVID-19 treatment. The underlying antiviral mechanisms could be related with interfering S-ACE2 interaction and preventing virus entry into cells. Moreover, alisol B 23-acetate also has anti-inflammation activities against coronavirus infection. With anti-viral and anti-inflammation activities, alisol B 23-acetate could be a potential therapeutic agent with the potentials for drug discovery to treat COVID-19, creating opportunity to fight the newly emerged coronavirus variants in the future.

Declaration of Competing Interest

The authors declare that they have no known competing financial interests or personal relationships that could have appeared to influence the work reported in this paper.

Acknowledgements

This work was supported by Areas of Excellence Scheme, Research Grant Council, Hong Kong SAR, China (No. AoE/P-705/16, JGS). The Health and Medical Research Fund (grant no. CID-HKU1-11, SFY), the Food and Health Bureau, Hong Kong SAR. Health@InnoHK, Innovation and Technology Commission, the Government of the Hong Kong Special Administrative Region. We thank Faculty Core Facility, Li Ka Shing Faculty of Medicine, the University of Hong Kong to supply Carl Zeiss LSM 800 for capturing confocal fluorescent images and BD LSR Fortessa for flow cytometry assay. We acknowledge Dr. Lin Xiang for the support the human PBMC.

Appendix A. Supplementary material

Supplementary data to this article can be found online at https://doi.org/10.1016/j.jare.2023.10.002.

References

[1] Peiris JSM et al. Coronavirus as a possible cause of severe acute respiratory syndrome. Lancet (London, England) 2003;361(9366):1319–25.
[2] Zaki AM et al. Isolation of a novel coronavirus from a man with pneumonia in Saudi Arabia. N Engl J Med 2012;367(19):1814–20.
[3] Chan JFW et al. Middle East respiratory syndrome coronavirus: another zoonotic betacoronavirus causing SARS-like disease. Clin Microbiol Rev 2015;28(2):465–522.
[4] Orgnaztion WH. Coronavirus Disease (COVID-19) Situation Reports. https://www.who.int/emergencies/diseases/novel-coronavirus-2019/situation-reports, 2020.
[5] Chan J-F-W et al. A familial cluster of pneumonia associated with the 2019 novel coronavirus indicating person-to-person transmission: a study of a family cluster. Lancet 2020;395(10223):514–23.
[6] Torjesen I. Covid-19: Omicron may be more transmissible than other variants and partly resistant to existing vaccines, scientists fear. BMJ 2021;375:n2943.
[7] Williamson EJ et al. Factors associated with COVID-19-related death using OpenSAFELY. Nature 2020;584(7821):430–6.
[8] Ghosh N, Nandi S, Saha I. A review on evolution of emerging SARS-CoV-2 variants based on spike glycoprotein. Int Immunopharmacol 2022:108565.
[9] Han P et al. Receptor binding and complex structures of human ACE2 to spike RBD from omicron and delta SARS-CoV-2. Cell 2022;185(4):630–640.e10.
[10] Mannar D et al. SARS-CoV-2 omicron variant: antibody evasion and cryo-EM structure of spike protein–ACE2 complex. Science 2022;375(6582):760–4.
[11] Gottlieb RL et al. Early remdesivir to prevent progression to severe Covid-19 in outpatients. N Engl J Med 2022;386(4):305–15.
[12] Ader F et al. Remdesivir plus standard of care versus standard of care alone for the treatment of patients admitted to hospital with COVID-19 (DisCoVeRy): a phase 3, randomised, controlled, open-label trial. Lancet Infect Dis 2022;22(2):209–21.
[13] Angamo MT, Mohammed MA, Peterson GM. Efficacy and safety of remdesivir in hospitalised COVID-19 patients: a systematic review and meta-analysis. Infection 2022;50(1):27–41.
[14] Cao B et al. A trial of lopinavir-ritonavir in adults hospitalized with severe Covid-19. N Engl J Med 2020;382(19):1787–99.
[15] Goulao B, Hood K, Dahly D. Statistical review of Hydroxychloroquine in patients with COVID-19: an open-label, randomized, controlled trial. 2020.
[16] Investigators T-R-C. Interleukin-6 receptor antagonists in critically ill patients with covid-19. N Engl J Med 2021;384(16):1491–502.
[17] Owen DR et al. An oral SARS-CoV-2 Mpro inhibitor clinical candidate for the treatment of COVID-19. Science 2021:eabl4784.
[18] Jayk Bernal A et al. Molnupiravir for oral treatment of Covid-19 in nonhospitalized patients. N Engl J Med 2021;386(6):509–20.
[19] Singh AK et al. An updated practical guideline on use of molnupiravir and comparison with agents having emergency use authorization for treatment of COVID-19. Diabetes Metab Syndr 2022;16(2):102396.
[20] Dai EY et al. Viral Kinetics of Severe Acute Respiratory Syndrome Coronavirus 2 (SARS-CoV-2) Omicron Infection in mRNA-Vaccinated Individuals Treated and Not Treated with Nirmatrelvir-Ritonavir. medRxiv, 2022: p. 2022.08.04.22278378.
[21] Wang Q et al. Antibody evasion by SARS-CoV-2 Omicron subvariants BA.2.12.1, BA.4 and BA.5. Nature 2022.
[22] Wang X et al. Effectiveness and safety research of Qingfei Paidu (QFPD) in treatment of COVID-19: an up-to-date systematic review and meta-analysis. Chin Med 2022;17(1):1–16.
[23] Li Y et al. Identification of phytochemicals in Qingfei Paidu decoction for the treatment of coronavirus disease 2019 by targeting the virus-host interactome. Biomed Pharmacother 2022;156:113946.
[24] Yang R et al. Chemical composition and pharmacological mechanism of Qingfei Paidu Decoction and Ma Xing Shi Gan Decoction against Coronavirus Disease 2019 (COVID-19): in silico and experimental study. Pharmacol Res 2020;157:104820.
[25] Banerjee S et al. Glycyrrhizin as a promising kryptonite against SARS-CoV-2: clinical, experimental, and theoretical evidences. J Mol Struct 2022:134642.
[26] Yi Y et al. Natural triterpenoids from licorice potently inhibit SARS-CoV-2 infection. J Adv Res 2022;36:201–10.
[27] Fiore C et al. Antiviral effects of Glycyrrhiza species. Phytother Res 2008;22(2):141–8.
[28] Zhong LLD et al. Potential targets for treatment of coronavirus disease 2019 (COVID-19): a review of Qing-Fei-Pai-Du-Tang and its major herbs. Am J Chin Med 2020;48(05):1051–71.
[29] Chen H et al. Therapeutic targets of oxidative/nitrosative stress and neuroinflammation in ischemic stroke: applications for natural product efficacy with omics and systemic biology. Pharmacol Res 2020;158:104877.
[30] Chen J et al. Protection against COVID-19 injury by qingfei paidu decoction via anti-viral, anti-inflammatory activity and metabolic programming. Biomed Pharmacother 2020;129:110281.
[31] Xu W et al. Pharmacokinetics and tissue distribution of five major triterpenoids after oral administration of Rhizoma Alismatis extract to rats using ultra high-performance liquid chromatography–tandem mass spectrometry. J Pharm Biomed Anal 2017;146:314–23.
[32] Jin H-G et al. A new triterpenoid from Alisma orientale and their antibacterial effect. Arch Pharm Res 2012;35(11):1919–26.
[33] Zhu H-C et al. Alisol B 23-acetate ameliorates azoxymethane/dextran sodium sulfate-induced male murine colitis-associated colorectal cancer via modulating the composition of gut microbiota and improving intestinal barrier. Front Cell Infect Microbiol 2021: p. 358.
[34] Meng Q et al. Protective effects of alisol B 23-acetate from edible botanical Rhizoma alismatis against carbon tetrachloride-induced hepatotoxicity in mice. Food Funct 2015;6(4):1241–50.
[35] Jiang Z-Y et al. A new triterpene and anti-hepatitis B virus active compounds from Alisma orientalis. Planta Med 2006;72(10):951–4.
[36] Han CW, Choi J-Y. Therapeutic effect of alisol acetate B on lipopolysaccharide-induced acute lung injury, in DSEPSIS, ACUTE RESPIRATORY DISTRESS SYNDROME, AND ACUTE LUNG INJURY. 2014, American Thoracic Society. p. A5726-A5726.

[37] Shin M-H et al. The anti-inflammatory effects of Alisma herb extract on allergic asthma mouse model. Mol Cell Toxicol 2014;10(2):197–206.
[38] Chan J-F-W et al. Simulation of the Clinical and Pathological Manifestations of Coronavirus Disease 2019 (COVID-19) in a Golden Syrian Hamster Model: Implications for Disease Pathogenesis and Transmissibility. Clin Infect Dis 2020;71(9):2428–46.
[39] Lu L et al. Neutralization of SARS-CoV-2 Omicron variant by sera from BNT162b2 or Coronavac vaccine recipients. medRxiv 2021.
[40] Yuan S et al. Clofazimine broadly inhibits coronaviruses including SARS-CoV-2. Nature 2021;593(7859):418–23.
[41] Hoffmann M et al. SARS-CoV-2 cell entry depends on ACE2 and TMPRSS2 and is blocked by a clinically proven protease inhibitor. Cell 2020;181(2):271–280.e8.
[42] Huang L et al. Conformational dynamics of the helix 10 region as an allosteric site in class A β-lactamase inhibitory binding. J Am Chem Soc 2020;142(32):13756–67.
[43] Lin X et al. IL-10-producing regulatory B cells restrain the T follicular helper cell response in primary Sjögren's syndrome. Cell Mol Immunol 2019;16(12):921–31.
[44] Yuan S et al. SREBP-dependent lipidomic reprogramming as a broad-spectrum antiviral target. Nat Commun 2019;10(1):120.
[45] Yuan S et al. Pathogenicity, transmissibility, and fitness of SARS-CoV-2 Omicron in Syrian hamsters. Science 2022;377(6604):428–33.
[46] Peng T et al. A rationally designed rhodamine-based fluorescent probe for molecular imaging of peroxynitrite in live cells and tissues. Chem Sci 2016;7(8):5407–13.
[47] Bhatia M, Moochhala S. Role of inflammatory mediators in the pathophysiology of acute respiratory distress syndrome. J Pathol: J Pathol Soc Great Britain and Ireland 2004;202(2):145–56.
[48] Blaser H et al. TNF and ROS crosstalk in inflammation. Trends Cell Biol 2016;26(4):249–61.
[49] Laforge M et al. Tissue damage from neutrophil-induced oxidative stress in COVID-19. Nat Rev Immunol 2020;20(9):515–6.
[50] Delorey TM et al. COVID-19 tissue atlases reveal SARS-CoV-2 pathology and cellular targets. Nature 2021;595(7865):107–13.
[51] Grant RA et al. Circuits between infected macrophages and T cells in SARS-CoV-2 pneumonia. Nature 2021;590(7847):635–41.
[52] Yeung ML et al. Soluble ACE2-mediated cell entry of SARS-CoV-2 via interaction with proteins related to the renin-angiotensin system. Cell 2021;184(8):2212–2228.e12.
[53] Cai Y et al. Distinct conformational states of SARS-CoV-2 spike protein. Science 2020;369(6511):1586–92.
[54] Li L et al. Structural basis of human ACE2 higher binding affinity to currently circulating Omicron SARS-CoV-2 sub-variants BA.2 and BA.1.1. Cell 2022;185(16):2952–2960.e10.
[55] Hong Q et al. Molecular basis of receptor binding and antibody neutralization of Omicron. Nature 2022;604(7906):546–52.
[56] Towler P et al. ACE2 X-ray structures reveal a large hinge-bending motion important for inhibitor binding and catalysis *. J Biol Chem 2004;279(17):17996–8007.
[57] Wang Q et al. Structural and functional basis of SARS-CoV-2 entry by using human ACE2. Cell 2020;181(4):894–904.
[58] Shang J et al. Structural basis of receptor recognition by SARS-CoV-2. Nature 2020;581(7807):221–4.
[59] Lan J et al. Structure of the SARS-CoV-2 spike receptor-binding domain bound to the ACE2 receptor. Nature 2020;581(7807):215–20.
[60] Shukla AK, Banerjee M. Angiotensin-Converting-Enzyme 2 and Renin-Angiotensin System Inhibitors in COVID-19: An Update. High Blood Pressure & Cardiovascular Prevention 2021;28(2):129–39.
[61] Ravichandran B et al. SARS-CoV-2 and hypertension. Physiol Rep 2021;9(11):e14800.
[62] Chen H et al. Alisol B 23-acetate attenuates CKD progression by regulating the renin–angiotensin system and gut–kidney axis. Therapeutic Adv Chronic Disease 2020;11.
[63] Matsuyama S et al. Efficient Activation of the Severe Acute Respiratory Syndrome Coronavirus Spike Protein by the Transmembrane Protease TMPRSS2. J Virol 2010;84(24):12658–64.
[64] Shereen MA et al. COVID-19 infection: Emergence, transmission, and characteristics of human coronaviruses. J Adv Res 2020;24:91–8.
[65] Zhao H et al. SARS-CoV-2 Omicron variant shows less efficient replication and fusion activity when compared with Delta variant in TMPRSS2-expressed cells. Emerging Microbes Infect 2022;11(1):277–83.
[66] Ou X et al. Characterization of spike glycoprotein of SARS-CoV-2 on virus entry and its immune cross-reactivity with SARS-CoV. Nat Commun 2020;11(1):1620.
[67] Cantuti-Castelvetri L et al. Neuropilin-1 facilitates SARS-CoV-2 cell entry and infectivity. Science 2020;370(6518):856–60.
[68] Bao L et al. The pathogenicity of SARS-CoV-2 in hACE2 transgenic mice. Nature 2020;583(7818):830–3.
[69] Imai M et al. Syrian hamsters as a small animal model for SARS-CoV-2 infection and countermeasure development. Proceedings of the National Academy of Sciences, 2020;**117**(28): 16587–16595.
[70] Askani E et al. Computed tomographic imaging features of COVID-19 pneumonia caused by the delta (B.1.617.2) and omicron (B.1.1.529) variant in a German nested cohort pilot study group. Tomography 2022;8:2435–49. doi: https://doi.org/10.3390/tomography8050202.
[71] Hojyo S et al. How COVID-19 induces cytokine storm with high mortality. Inflam Regenerat 2020;40(1):37.
[72] Tang Y et al. Cytokine storm in COVID-19: the current evidence and treatment strategies. Front Immunol 2020;11.
[73] Gattinoni L et al. COVID-19 does not lead to a "typical" acute respiratory distress syndrome. Am J Respir Crit Care Med 2020;201(10):1299–300.
[74] Pacha O, Sallman MA, Evans SE. COVID-19: a case for inhibiting IL-17? Nat Rev Immunol 2020;20(6):345–6.
[75] Cao X. COVID-19: immunopathology and its implications for therapy. Nat Rev Immunol 2020;20(5):269–70.
[76] Kridin K et al. Risk of COVID-19 infection, hospitalization, and mortality in patients with psoriasis treated by interleukin-17 inhibitors. J Dermatol Treat 2022:1–7.
[77] Conti P et al. Induction of pro-inflammatory cytokines (IL-1 and IL-6) and lung inflammation by Coronavirus-19 (COVI-19 or SARS-CoV-2): anti-inflammatory strategies. J Biol Regul Homeost Agents 2020;34(2):1.
[78] Cavalli G et al. Interleukin-1 blockade with high-dose anakinra in patients with COVID-19, acute respiratory distress syndrome, and hyperinflammation: a retrospective cohort study. The Lancet Rheumatology 2020;2(6):e325–31.
[79] Bastard P et al. Autoantibodies against type I IFNs in patients with life-threatening COVID-19. Science 2020;370(6515).
[80] Karki R et al. Synergism of TNF-α and IFN-γ triggers inflammatory cell death, tissue damage, and mortality in SARS-CoV-2 Infection and CYTOKINE shock syndromes. Cell 2021;184(1):149–168.e17.
[81] Ghosh R et al. Neutralization of IL-17 and treatment with IL-2 protects septic arthritis by regulating free radical production and antioxidant enzymes in Th17 and Tregs: an immunomodulatory TLR2 versus TNFR response. Cell Immunol 2021;370:104441.
[82] Saheb Sharif-Askari N et al. Upregulation of oxidative stress gene markers during SARS-COV-2 viral infection. Free Radic Biol Med 2021;172:688–98.
[83] Radzikowska U et al. Distribution of ACE2, CD147, CD26, and other SARS-CoV-2 associated molecules in tissues and immune cells in health and in asthma, COPD, obesity, hypertension, and COVID-19 risk factors. Allergy 2020;75(11):2829–45.
[84] Wu A et al. Genome composition and divergence of the novel coronavirus (2019-nCoV) originating in China. Cell Host Microbe 2020;27(3):325–8.
[85] Ziegler CGK et al. SARS-CoV-2 receptor ACE2 is an interferon-stimulated gene in human airway epithelial cells and is detected in specific cell subsets across tissues. Cell 2020;181(5):1016–35.
[86] Shen X-R et al. ACE2-independent infection of T lymphocytes by SARS-CoV-2. Signal Transduct Target Ther 2022;7(1):83.
[87] Vankadari N, Wilce JA. Emerging COVID-19 coronavirus: glycan shield and structure prediction of spike glycoprotein and its interaction with human CD26. Emerging Microbes Infect 2020;9(1):601–4.
[88] Pushkarsky T. et al. CD147 facilitates HIV-1 infection by interacting with virus-associated cyclophilin A. Proc Natl Acad Sci, 2001;**98**(11): p. 6360-6365.
[89] Zhang Y et al. A UFLC/MS/MS method for simultaneous quantitation of alisol A and alisol B 23-acetate from Alisma orientale (Sam.) Juz. in rat plasma. Asian J Pharm Sci 2014;9(5):279–85.
[90] Meng Q et al. Alisol B 23-acetate protects against non-alcoholic steatohepatitis in mice via farnesoid X receptor activation. Acta Pharmacol Sin 2017;38(1):69–79.